DRAFT **NIST Special Publication 1227**

Performance Metrics and Test Methods for Robotic Hands

Joe Falco
Karl Van Wyk
Elena Messina

This publication is available free of charge from:
https://doi.org/10.6028/NIST.SP.1227-draft

National Institute of
Standards and Technology
U.S. Department of Commerce

DRAFT **NIST Special Publication 1227**

Performance Metrics and Test Methods for Robotic Hands

Joe Falco
Karl Van Wyk
Elena Messina
Intelligent Systems Division
Engineering Laboratory

This publication is available free of charge from:
https://doi.org/10.6028/NIST.SP.1227-draft

October 2018

U.S. Department of Commerce
Wilbur L. Ross, Jr., Secretary

National Institute of Standards and Technology
Walter Copan, NIST Director and Undersecretary of Commerce for Standards and Technology

National Institute of Standards and Technology Draft Special Publication 1227
Natl. Inst. Stand. Technol. Draft Spec. Publ. 1227, 65 pages (October 2018)
CODEN: NSPUE2

This publication is available free of charge from:
https://doi.org/10.6028/NIST.SP.1227-draft

This is a working document from a NIST led working group under the Institute of Electrical and Electronics Engineers (IEEE) Robotic Hands Grasping and Manipulation (RHGM) Technical Committee with periodic updates based on public comment. It serves as an archive for future community concensus based standards development work. Opportunities to comment on this document will be announced using robotics community portals such as rhgm.org and robotics-worldwide. Comments should be communicated using the robot-performance@nist.gov mail list (see https://email.nist.gov/mailman/listinfo/robot-performance to sign up). Use "Benchmark" as the subject line when submitting comments for this document. All comments are subject to release under the Freedom of Information Act (FOIA).

Abstract

Increasing the flexibility and general-purpose applicability of robots is a longstanding goal. Several avenues of research are addressing these goals, ranging from integration of multiple sensors to allow robots to perceive their surroundings and adapt accordingly, to more sophisticated control algorithms that enable robots to re-plan based on current status, to development of more dexterous means of manipulating objects. As part of the manipulation thrust, there has been a recent increase in the development of robotic hands. Inspired by nature, these end effectors hold potential for allowing robots to pick up and manipulate a broader range of objects, without requiring customized end-of-arm tooling or grippers. With this rapidly-growing number of robot hands with diverse designs, there is a need to capture their individual competencies and characteristics under a unified framework. In addition to knowledge of basic hand characteristics such as the number of fingers, degrees of freedom, and degrees of actuation, performance metrics can provide valuable insight into not only the raw traits of the technology, but also their task and function-level performance capabilities. These measures can then be used to help match capabilities to end-user needs as well as provide researchers and developers insight for improving their hardware and software designs.

Key words

Benchmarking; Grasping; Manipulation; Robotics; Performance; Measures; Test Methods.

Table of Contents

List of Tables

List of Figures

1. Introduction

Mechanisms inspired by the vastly agile grasping capabilities and dexterity of human hands are being developed to enhance the flexibility and general-purpose usability of robotic systems. At this point in time, there are varying levels of anthropomorphism in the designs of robotic hands. Although the term "hand" is applied to this general category of end-effectors, not all of them consist of a palm with five articulated digits, including opposable thumbs. Some designs attempt to reproduce many aspects of human hands (bone and tendon structure) resulting in very realistic mechanisms of great complexity (e.g., [3, 4]) with only a few degrees of freedom. These designs are usually classified as being part of the hand category. The intended application for these hands also varies considerably. Their uses include serving as human prostheses, or as parts of robots that perform service, assistive, military, medical, or industrial functions.

To design relevant performance metrics and methods for characterizing robotic hands, it helps to understand the contextual or application-specific issues surrounding robotic grasping and manipulation. Characterization of a robotic hand should not be thought of in terms of a single value or dimension. Rather, a full characterization that involves a range of metrics is needed to guide selection of appropriate hands for a particular application and to direct research and development advancements.

Regardless of the actual task, any grasping and manipulation problem can be broken down into its first principles: kinematics and kinetics, or more simply, motion and effort. Kinetics are the forces acting on bodies or particles that are responsible for causing their motion. Any kinetic metric or test method will be evaluating force, torques, and any other measure of effort, such as electrical current. Kinematics is the geometry of motion of bodies or particles, disregarding the forces that cause such motion. Therefore, any kinematic metric or test method will be concerned with evaluating positions, velocities, or accelerations of bodies, parts, or particles, and will typically be expressed in units of length and time. Evaluation areas of interest include palms, fingers, points of contact, or parts under grasp. Building test methods using this first principles approach will ultimately lead to relevant performance capture, and will span from lower-level capabilities including primitive sensing and control to higher-level capabilities including manipulation, perception, and decision making.

When evaluating the capabilities of a robotic hand, performance tests should be agnostic to the other system components such as the robot arm and perception system. While it is possible to access data directly from a robotic hand and derive the defined metrics, these measurements would be based on the inherent properties of the system under test. Therefore, independent measurement systems must be developed to support testing to allow for comparative metrics between systems to establish extrinsic ground truths.

This publication contains a series of elemental metrics that were identified through a combination of literature reviews, workshops, and interactions with participants in a metrics working group formed under the Institute of Electrical and Electronic Engineers (IEEE) Robotics and Automation Society Robotic Hand Grasping and Manipulation Technical Committee. Each section defines a metric and a test method. The test method describes the test setup, artifacts, measurements, and guidance for analysis of the measurements. A listing of the test methods and associated measurement instrumentation is shown in Table 1. Additionally, many sections contain an example implementation[1] of the test method using the two robotic hands shown in Figure 1 as well as an array of integrated sensor systems and control algorithms. Appendices provide background and additional information about grasp metrics, analysis of grasping tasks, and artifact design. The National Institute of Standards and Technology (NIST) continues to develop, where possible, lower-cost alternatives to the artifact designs.

Test Method	Measurement Instrument
Finger Strength	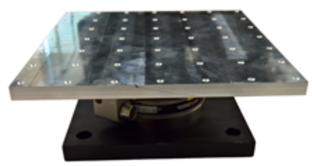 6- Axis Load Cell
Touch Sensitivity	
Finger Force Tracking	
Force Calibration	
Grasp Strength	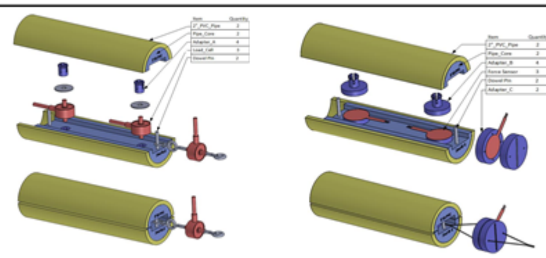 Split Cylinder Artifact
Slip Resistance	
Grasp Efficiency	
Cycle Time	
In-Hand Manipulation	 Motion Tracking System
Object Pose Estimation	

Table 1. Listing of test methods and associated measurement instruments

[1]Example implementations are produced to demonstrate use of the test method.

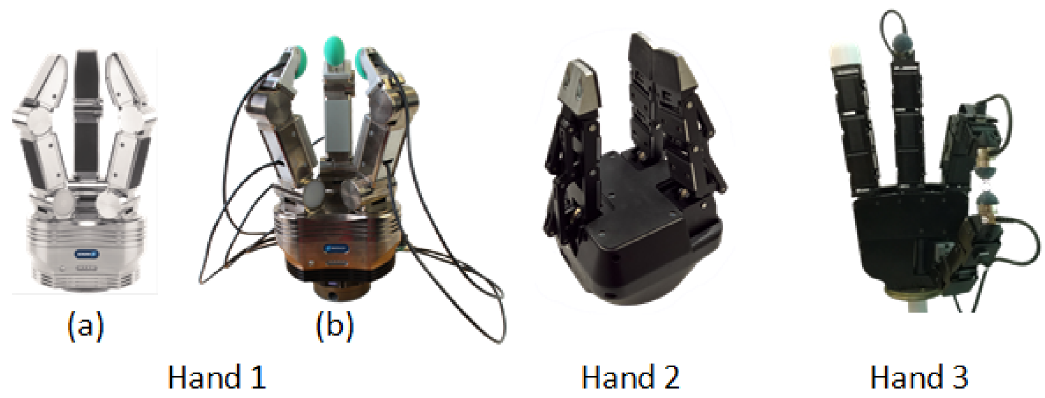

Fig. 1. Robot hands used to verify test methods: Hand 1(a) - Schunk Dexterous Hand, a three-fingered, 7 degree-of-actuation robotic hand with Weiss Robotics resistance based tactile sensors; Hand 1(b) - Schunk Dexterous Hand retrofitted with bio-inspired impedance based tactile sensors; Hand 2 - Robotiq Adaptive Gripper with current sensing; Hand 3 - Allegro Hand retrofitted with six-axis load cells at fingertips

2. Towards Standardized Benchmarks for Robotic Hands

,Robotic hands are an integrated mechatronic system of sensors, motors, and control algorithms ranging from three-fingered to five-fingered anthropomorphic designs having both fully- and under- articulated joints, sometimes with built-in compliance. Designs incorporate a variety of sensing technologies including simple current sensing at the drive motors, load cells, barometers, hydrophones, pressure transducers, electrodes, cameras, and tactile arrays. Depending on the sensory layouts and mechanical implementation, tactile sensing capabilities can include the ability to resolve point of contact, directionality and magnitude of contact forces as well as other sensing modalities such as vibration and temperature. Control algorithms use these signals to incorporate position, velocity, and force control schemes. This wide scope of performance characteristics requires a modular set of performance metrics and associated test methods that can be chosen based on a defined set of grasp types the hand can perform, as well as a scheme for classifying a hand that includes sensing and control capabilities. Also needed are a common set of test objects (artifacts) to be used along with the test methods. A framework for benchmarking the performance of robotic hands is shown in Figure 2

Grasp taxonomies for the human hand have been developed towards the understanding of grasps that humans commonly use in everyday tasks. Cutkosky [5] performed a study of the grasps used by machinists in a small batch manufacturing operation and developed a taxonomy of grasps to provide insights for the design of versatile robotic hands for manufacturing. Feix et al. [6] derive a taxonomy of grasps based on a literature review of 14 human grasp studies (including Cutkosky's) from both the robotics and medical communities. The knowledge of these grasp taxonomies has been applied to the design of robotic

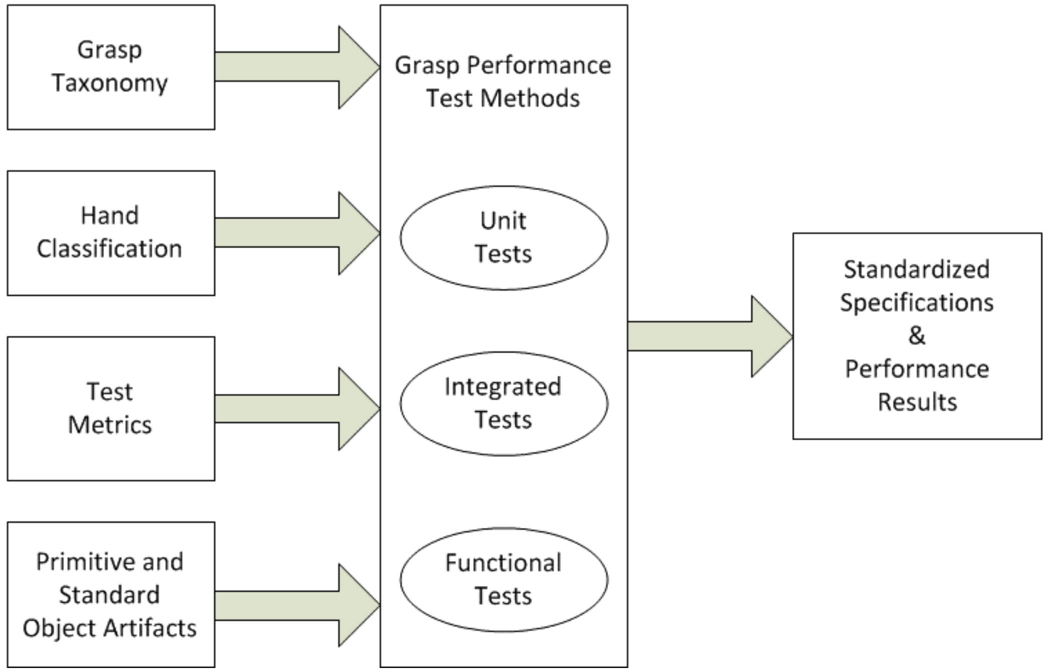

Fig. 2. Framework for standardized performance benchmarking of robotic hands

and prosthetic hands and provides a basis for describing the grasp types that a hand can perform.

Performance tests should encompass general grasping tasks as defined in Appendix B and be comprised of unit, integrated, and functional test methods. When evaluating the capabilities of a robotic hand, unit and integrated performance tests should be agnostic to the other system components such as the robot arm and perception system. While it is possible to access data directly from a robotic hand and derive the defined metrics, these measurements would be based on the inherent properties of the system under test. Therefore, independent measurement systems must be developed to support testing to allow for comparative metrics between systems without effects, such as force accuracies and data latencies.

Unit performance characteristics include kinematic properties such as volumetric capabilities and grasp configurations with associated maximum force capabilities. At the very basic level, primitive geometries such as spheres, cylinders, and cubes can be used to characterize the volumetric capabilities of a hand and maximum pinch and grasp forces can be determined at the bounds of these primitive volumetric capabilities. Individual finger tests can be performed to determine the positional accuracy and repeatability of the finger as well as velocity and acceleration characteristics. Sensors can be tested at their stock sensing modalities for properties such as resolution and sensitivity. For example, in the case of tactile sensors, desired characteristics might include normal and shear sensing capabilities, as well as the ability to resolve the direction for forces and spatial resolution.

Integrated system characteristics include tests to evaluate the ability of a hand to withstand external forces while maintaining a good level of grasp efficiency and the ability to make initial contact with an object with minimal disturbance to the object. In addition, tests are needed to characterize the integration of a sensor system. For example, one test is defined to characterize the latency of a finger's motion to feedback from a tactile sensor. Another test characterizes the performance of a hand to adjust grasp forces to prevent slip due to changes in external forces on the object.

Functional tests which include the added performance characteristics of a robot arm and perception system can be standardized if they are defined generically to meet the requirements of an application space or to evaluate the capabilities of more than one robotic hand technology for a known application (e.g., benchmarking). These generic functional assessments of the hand's performance follow unit and integrated testing. Finally, functional tests should be performed within the actual application space for final performance verification.

In summary, standardized performance benchmarks for robotic hands offer the benefits of an "honest broker" to characterize system performance. The results of such evaluations and benchmarks help to match capabilities to end-user needs, as well as to help developers improve their product designs[2]. To date, benchmarks to assess the results of grasp research are primarily qualitative measures. However, there is evidence, as described in Appendix A, of quantitative assessments of grasping research results scattered across the community. Standardized benchmarks will require a framework for matching the grasp types that a system under test can perform, as well as its sensing and control capabilities to the right set of unit and integrated performance tests in order to perform a thorough evaluation of a robotic hand system.

It is hoped that researchers will begin using these test methods and communicate the performance test results of robotic hands in scholarly publications. The impact of different mechanical designs, sensors, and control algorithms can be quantified using these test methods. The metrics provided herein will provide a common language for comparing different hand designs and will strengthen the progress of development and deployment of more-capable robotic hands. Experiences in applying these test methods will serve to improve them over time. The evolved versions of these test methods can then be submitted to a standards development organization to go through the process of consensus review and balloting.

This publication is structured as follows. We begin with a series of elemental metrics that were identified through a combination of literature reviews, workshops, and interactions

[2]When using these tools to compare the performance of robot hands, always keep in mind the intended application. Hands evaluated to yield high strength characteristics with lower control and manipulation characteristics may be better suited for heavy-lifting applications, where hands with less strength and better control and manipulation characteristics are better suited for fine dexterity applications.

with participants in a metrics working group formed under the Institute of Electrical and Electronic Engineers (IEEE) Robotics and Automation Society Robotic Hand Grasping and Manipulation Technical Committee. NIST has created a web site to collect these metrics and provide test method details and data so that the community can experiment with them and provide feedback for improvement. For each metric, there is a discussion, followed by a test method that has been developed and implemented by NIST. Artifacts and procedures are described, along with example data collected by NIST. Artifact designs are available for download from a NIST site. The designs are intended to provide means of replicating the test methods without requiring expensive infrastructure or complex fabrication procedures. NIST continues to develop, where possible, lower-cost alternatives to the artifact designs. Links to the designs and the datasets collected through these test methods are provided within each sub-section. Appendices provide additional information that is relevant to grasp performance. Appendix A presents a brief overview of existing literature on grasp metrics. Further details about how a grasping task can be analyzed are found in Appendix B. The artifacts used in the test methods are described in Appendix C. Finally, Appendix D provides guidance on determining the sample size for conducting statistically significant experiments.

3. Finger Strength

3.1 Metric

3.1.1 Definition

Finger strength is a kinetic measure of the maximum force a robotic finger can impose on its environment. This measure relates to the overall strength of the hand during grasping or manipulation. The reasons for measuring strength on a single finger are two-fold:

1. Grasping and manipulation can occur with any number of fingers which means that the most independent measure of strength would be finger strength.

2. There can be inherent variability in finger strength across different fingers even in cases where they are mechanically equivalent.

3.1.2 Dependencies

Strength is a function of the finger's actuator capabilities, motion controllers, mechanical design, and finger-to-object configuration.

3.2 Test Method

3.2.1 Measurement Instrument

1. Calibrated load cell for measuring force in three dimensions (F_x, F_y, F_z) or single axis load cell for measuring force in one dimension.

2. Required data acquisition hardware and software.

Note: Attaching a rigid column to these sensors for finger interaction can help avoid unwanted hand-to-sensor collisions.

3.2.2 Description

Of the finger strength dependencies, only the finger-to-object configuration is a test variable. Using desired finger-object configuration, position the finger under test just above the force sensor and verify a zero-force reading. Under position control, the finger is then commanded to close completely which should induce control saturation. The finger-to-object configuration for benchmarking occurs when the induced moment arm from making contact is at its maximum, which means the maximum attainable contact force will be at a minimum for the finger under test. For most hand designs, this occurs when a finger is fully extended and all finger links are extended in the same direction as shown in Figure 3. This configuration measures the global minimum finger strength (i.e., any other configuration would yield higher finger strength.) In the case of using a single-axis load cell, slight adjustment should be made to this finger-object configuration such that the contact force of the finger is normal to force sensor contact surface. This prevents dispersing contact force in directions that are not measurable. This test method can be applied to additional finger-to-object configurations.

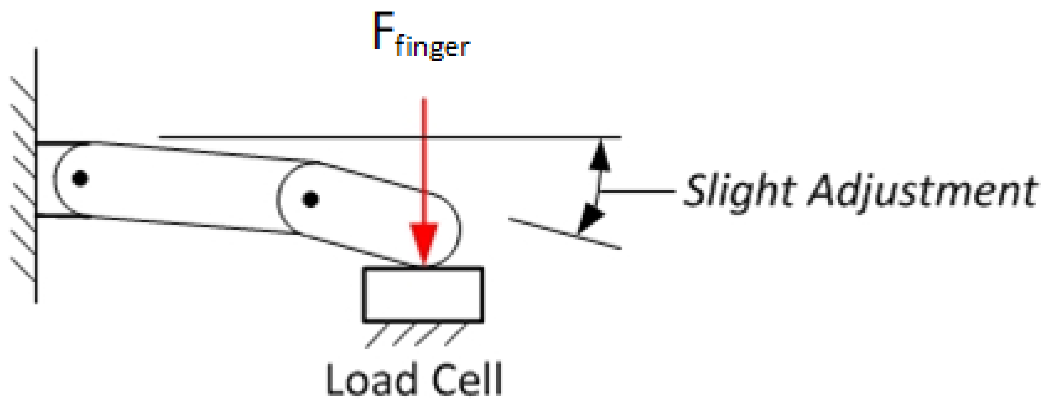

Fig. 3. Finger Strength Test Setup

3.2.3 Performance Measures

The fingertip contact force magnitude, F_{finger}, should be computed as:

$$F_{finger} = \sqrt{\left(F_x^2 + F_y^2 + F_z^2\right)} \tag{1}$$

for each set of force readings given by the load cell. Next, the contact force magnitude from the quasi-static force region (see Figure 4) should be extracted for each load cycle, and then averaged to yield the maximum finger strength, $F_{finger,max}$. The resultant contact force is extracted from the quasi static contact force profile and the peak dynamic contact force is ignored. This measure eliminates the effects introduced through contact momentum, yielding the steady state strength of the finger.

3.2.4 Test Setup and Procedure

1. Position the robotic finger in a fully-extended position as depicted in Figure 3.

2. Once in this configuration, the finger is positioned just above the external force sensor with verification of zero force.

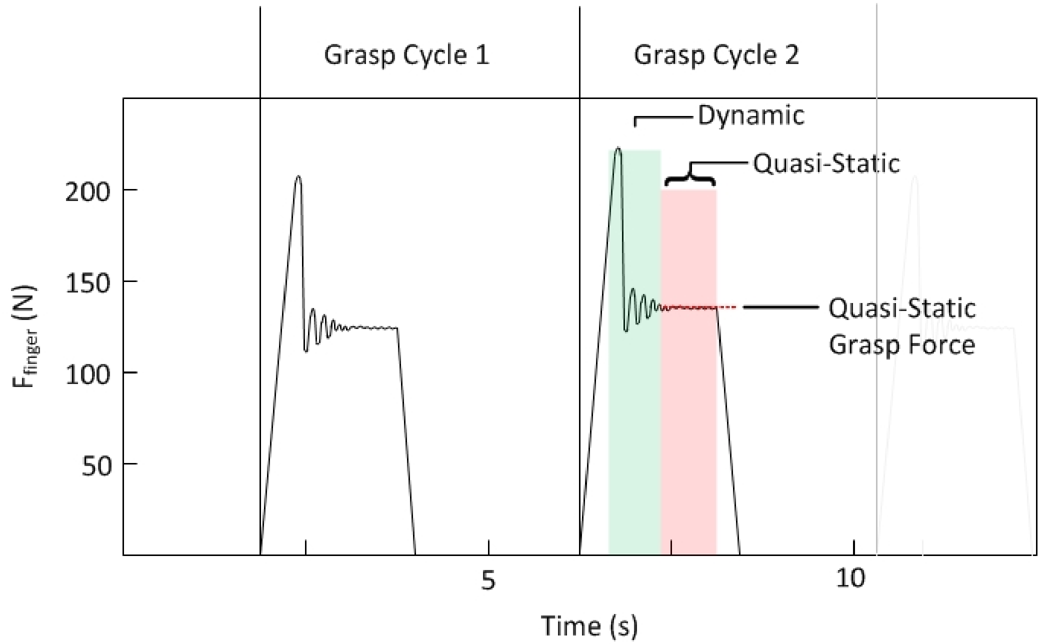

Fig. 4. Depiction of dynamic and quasi-static force regions during finger load cycles

3. Under position control, the finger is then commanded to close completely to induce control saturation at a fully extended configuration.
4. Once contact has been established for a few seconds, the finger is retracted to its start position.
5. Repeat the process for the desired sample size (see Appendix D for guidance) per finger tested.
6. Record force sensor data throughout the test.
7. Calculate the performance measures.

3.2.5 Example Implementation

NIST performed a series of tests using the finger force metric and test method for Hand 1 and Hand 2. In the case of Hand 1, the resistance sensing fingertips were used since they where purchased as an option for Hand 1 and would most likely withstand the maximum forces applied by each finger. The setups for these example implementations are shown in Figure 5. A 6-axis load cell with a rigid column is used to collect force measures at 3000 Hz. In these tests, the hands are mounted to a robot manipulator for ease of positioning. All robot fingers were tested for 32 cycles. Figure 6 is a plot of the finger force samples from a finger on NIST Hand 1. Conducting this test method across all fingers on both NIST Hand 1 and NIST Hand 2 yields $F_{finger,max}$ as shown in Figure 7.

Data from example test implementation

Data File Archive:	http://www.nist.gov/el/isd/upload/Finger-Strength.zip
Data Files:	Hand[Number]/Finger_[Number]
File Format:	ASCII, comma delimited
Data Values:	F_x, F_y, and F_z (one set per line)
Units:	Newtons
Data Sample Rate:	3 kHz

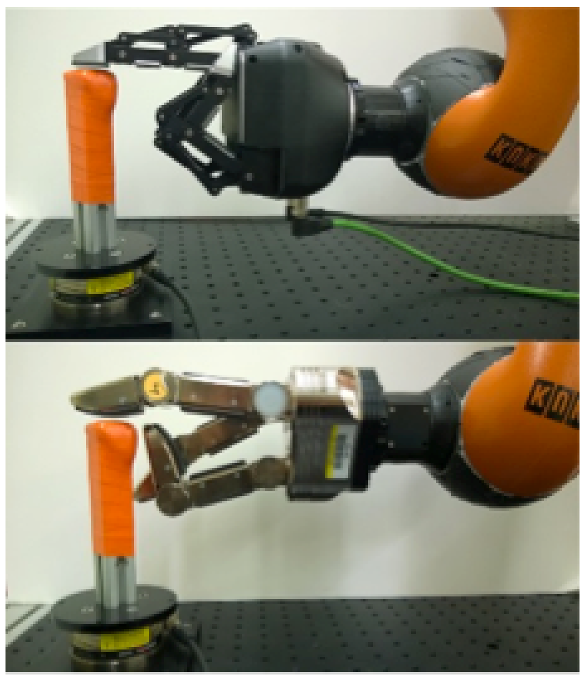

Fig. 5. Fingertip force test setup with NIST Hand 2(Top) and Hand 1 (Bottom) with resistance sensing fingertips tested using a 6-axis load cell. Fingers under test are positioned such that contact takes place at the fingertip with the finger fully extended and perpendicular to the palm.

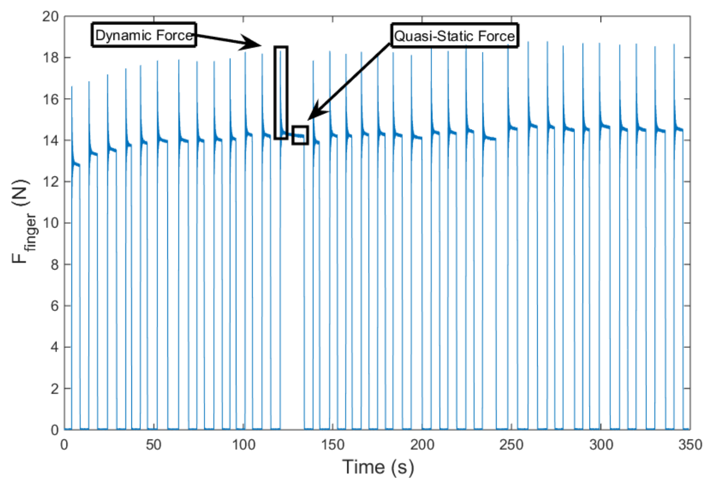

Fig. 6. Fingertip contact forces emitted by NIST Hand 1, Finger 1 during repeated testing.

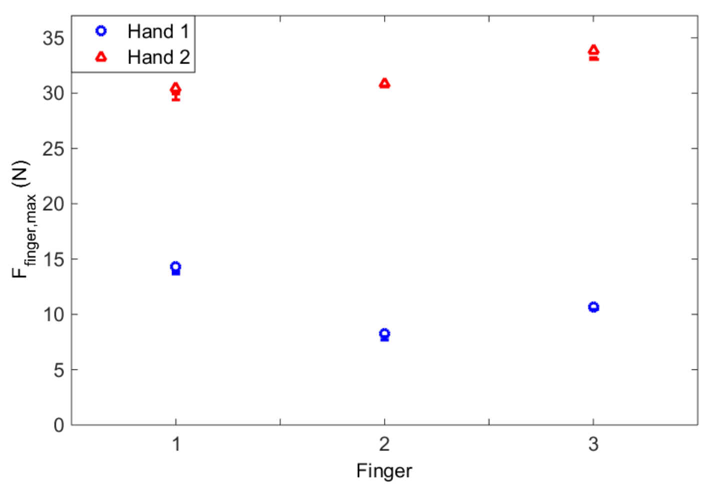

Fig. 7. $F_{finger,max}$ exerted by each finger for NIST Robot Hand 1 and Hand 2.

4. Grasp Strength

4.1 Metric

4.1.1 Definition

Grasp strength is a kinetic measure of the maximum force a robotic hand can impose on an object. This measure will yield information regarding a hand's payload capabilities for various object sizes as well as its limits in resisting pulling or pushing forces during a grasp operation.

4.1.2 Dependencies

Grasp strength is a function of the hand's actuator capabilities, motion controllers, mechanical design, grasp configuration, and object size.

4.2 Test Method

4.2.1 Measurement Instrument

1. Single axis load cells for one-dimensional force measurement F_i where i=1,2,. . . ,n and n is the total number of load cells
2. Split cylinder artifacts (see Appendix C)
3. Required data acquisition hardware and software.

4.2.2 Description

Of the grasp strength dependencies, only the grasp configuration and object size are assumed controllable. For this test, two common grasp types are chosen for investigation – pinch and wrap. The pinch grasp allows for measuring performance associated with precision grasping while the wrap grasp allows for measuring performance associated with power grasping. Split cylinder artifacts of different diameters are used to measure the internal force transmission of a grasp. Multiple cylinder diameters should be used to create a spread of performance results.

Different split cylinder artifact orientations can be used for performing wrap grasp tests:

1. In the 0° orientation, the load cell axis is parallel with the palm surface.
2. In the 90° orientation, the load cell axis is perpendicular to the palm surface.

These orientations under a wrap grasp are shown in Figure 8. Taking force measurements in two orthogonal directions provides a better approximation of a resultant internal force measurement since this artifact design only measures force in one direction.

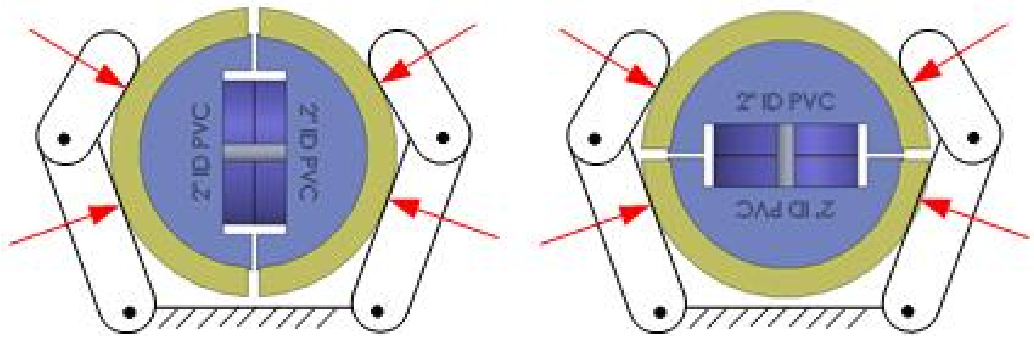

Fig. 8. A split cylinder artifact in the 0° (left) and 90° (right) orientations.

4.2.3 Performance Measures

For each set of instantaneous force readings, add forces across all load cells since they are in-line to yield a total grasp force F_{total},

$$F_{total} = \sum_{i=1}^{n} F_i \tag{2}$$

Next, the quasi-static force for each grasp cycle (see Figure 9) should be extracted for each artifact orientation and size. Quasi-static grasp forces are chosen for evaluation as they remove impact effects and give a more accurate estimate of the true strength of the hand. Given these quasi-static grasp forces, compute the force mean and 95 % confidence intervals for each artifact orientation (0° and 90°).

The final grasp force measure, F_{grasp}, is determined by computing the L_2 norm of the two means (one per orientation), the two lower bounds, and two upper bounds of the confidence intervals. These values approximate the mean resultant internal force magnitude (F_{grasp}), and its uncertainty.

Note: the confidence interval is calculated separately on the 0° and 90° grasp forces, before computing the L2 norm since the two data sets are independent test measures requiring repositioning of the split cylinder test artifact.

4.2.4 Test Setup and Procedure

1. Select different sized split cylinder artifacts to create a spread of performance results.
2. Grasp a split cylinder test artifact to achieve maximum force at the 0° orientation with the robotic hand under test, constraining the artifact to prevent movement when the test grasp is released.
3. Under position control, command the hand to open completely

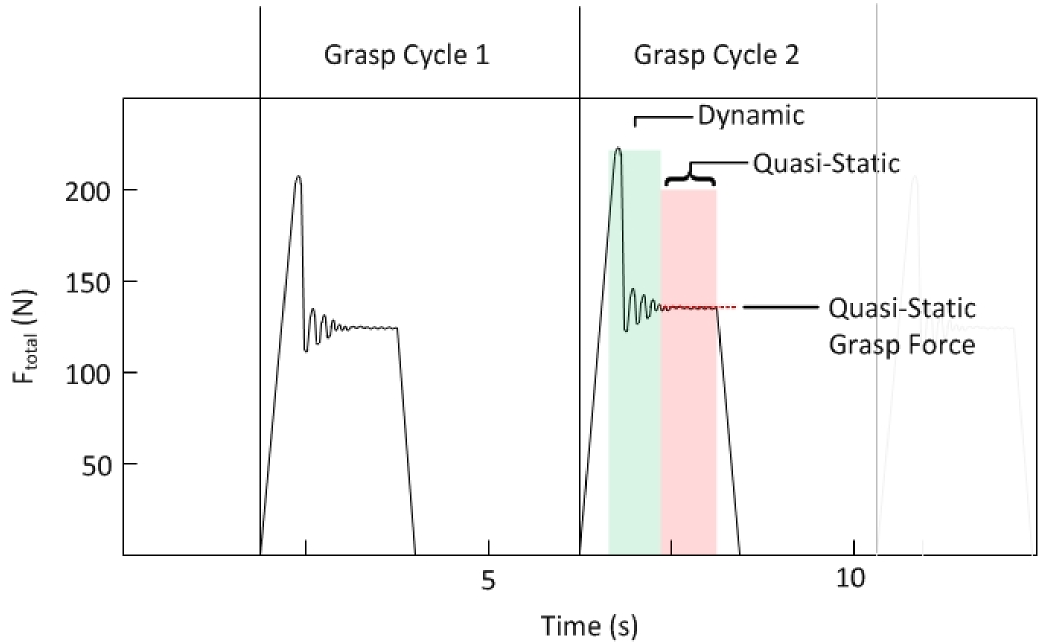

Fig. 9. Depiction of dynamic and quasi-static force regions during grasp cycles.

4. Under position control, command the hand to close completely to induce control saturation producing the maximum force closure grasp.

5. Once maximum force closure is established for a few seconds, the hand is retracted to its start position in the form closure grasped state with minimal force applied.

6. Repeat the process for the desired sample size (see Appendix D for guidance) for each split cylinder orientations and size. Note that summing the 0° and 90° orientation forces is optional depending on the hand design. In some cases, the non-dominate orientation forces can be determined to be negligible.

7. Record force sensor data throughout the test.

8. Calculate the performance measures.

Next, extract the quasi-static force for each grasp cycle (see Figure 9) for a particular artifact orientation and size. Quasi-static grasp forces are chosen for evaluation as they remove impact effects and give a more accurate estimate of the true strength of the hand. Given these quasi-static grasp forces, compute the force mean and 95% confidence intervals for each artifact orientation (0° and 90°). Note: for improving repeatability of force measurement, the artifact can be placed on a marked, cross-sectional template on a table with the hand rigidly mounted to grasp the artifact from the side. After one grasp cycle, the artifact could be re-positioned to the marked template.

4.2.5 Example Implementation

NIST performed a series of tests using the grasp strength metric and test method for Hand 1 and Hand 2. In the case of Hand 1, the resistance sensing fingertips were used since they where purchased as an option for Hand 1 and would most likely withstand the maximum forces encountered during grasp strength testing. An earlier prototype of the NIST split cylinder artifact that was designed with 50 mm and 80 mm diameter printed ABS plastic was used (Figure 10). This artifact housed two single-axis load cells to capture internal force transmission by the grasp. Force data was captured from two load cells at 3 kHz while fully opening and closing each robotic hand around each artifact 32 times for the 0° and 90° orientations.

A data plot of F_{total}, the sum of the two load cells throughout the 32 grasp cycles, is shown in Figure 11. The mean quasi-static grasp forces were extracted for each data set. Next, the mean and 95% confidence intervals for the force data collected in both orientations (0° and 90°) and the L_2 norms are computed for both hands. The results are shown for Hand 1 and Hand 2 in Table 2.

Data from example test implementation

Data File Archive:	http://www.nist.gov/el/isd/upload/Grasp-Strength.zip
Data Files:	Hand 1/C[cylinder diameter]_[Orientation] Hand 2/C[cylinder diameter]_[Orientation]
File Format:	ASCII (American Standard Code for Information Interchange), comma delimited
Data Values:	F1 and F2 (one set per line)
Units:	Newtons, Millimeter
Data Sample Rate:	3 kHz

	Hand 1 F_{grasp} (N)		Hand 2 F_{grasp} (N)	
Cylinder Diameter (mm)	Mean	95% Confidence Interval	Mean	95% Confidence Interval
50	47.0219	[44.366, 49.468]	118.983	[101.264, 137.843]
80	76.1081	[70.003, 84.323]	92.968	[84.811, 100.669]

Table 2. Mean and 95% confidence intervals of the internal grasp force for Hand 1 and Hand

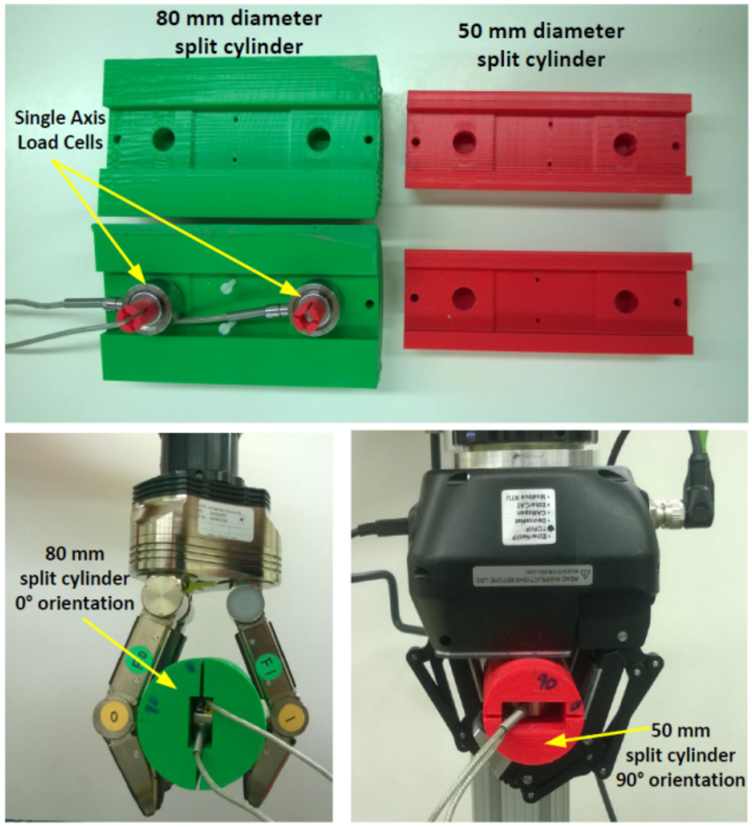

Fig. 10. Prototype 80 mm and 50 mm diameter split cylinder configurations for determining grasp forces (top). Grasp strength on NIST Hand 1 using 80 mm split cylinder at 0°, the dominant orientation for this hand (bottom left), and on Hand 2 using 50 mm prototype split cylinder at 90°, the dominant orientation for this hand(bottom right).

5. Slip Resistance

5.1 Metric

5.1.1 Definition

Slip resistance is a kinetic measure of a robotic hand's ability to resist slip. The focus of this metric is to investigate the inherent surface friction properties of the hand. With higher friction coefficients, robotic fingers will possess wider friction cones at the areas of contact with an object. This behavior would ultimately allow friction forces to contribute to the overall grasping effort, yielding greater resistance to slipping and generally enhanced energy efficiency during the grasping operation.

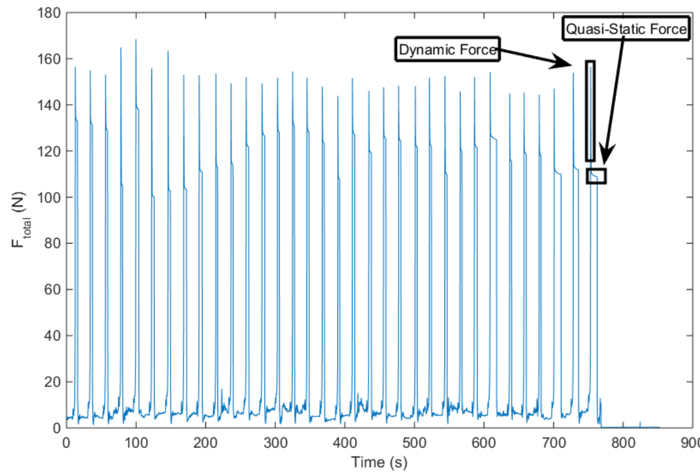

Fig. 11. Force data for Hand 2 wrap grasping the 50 mm prototype split cylinder in the 90° orientation.

5.1.2 Dependencies

Slip resistance depends on the hand's: actuator capabilities, motion controllers, mechanical design, grasp configuration, object size, and object surface properties.

5.2 Test Method

5.2.1 Measurement Instrument

1. Split cylinder artifacts (see Appendix C) or equivalent Standard ASTM D2665 polyvinyl chloride (PVC) pipe segments. Note: International PVC pipe standards could be selected to promote global adoption.

2. Single axis load cell for measuring force in one dimension.

3. Required data acquisition hardware and software.

4. A mechanism for providing a controlled increasing force along the axial direction to the pipe segment.

5.2.2 Description

Of the slip resistance dependencies, only the grasp configuration, object size, and object surface properties are assumed controllable. Given this large performance search space, some variables are fixed to make testing more tractable while still providing useful results. Specifically, the wrap force closure grasp on a cylindrical artifact was chosen to investigate slip resistance capabilities under maximum power and highest number of hand-to-object points of contact. Furthermore, use of a cylindrical shape under a wrap grasp eliminates the undesirable behavior of object-to-finger locking. ASTM D2665 PVC pipe is selected for the artifact for the following reasons:

1. The cylindrical pipe comes in a variety of standard diameters with dimensions that are compatible with robotic hand volumetric capabilities.

2. The surface properties of these pipes are relatively consistent. The general setup for this test is shown in Figure 12.

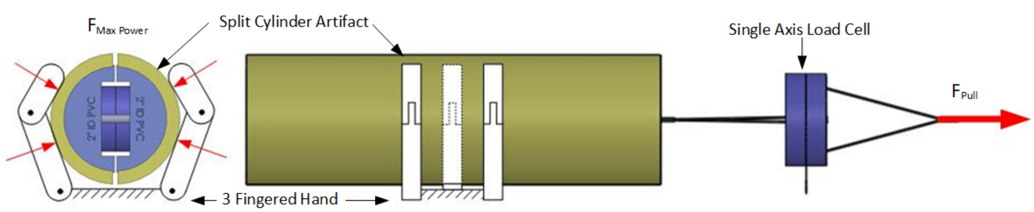

Fig. 12. Depictation of a three finger wrap grasp on a cylindrical artifact under maximum power $F_{MaxPower}$ with the cylinder subjected to an axial pull force F_{Pull}

.

5.2.3 Performance Measures

The measure of interest in this test is the maximum obtainable pull force before gross slip of a given hand and pipe size under a full-force wrap grasp. For each test cycle, record the pull force, F_{pull}, over time. Extract the maximum pull force, $F_{pull,max}$, from the force/time plot as shown in Figure 13. Calculate the mean and 95% confidence intervals for each pipe diameter size. Note that periodically during the pull force ascent, there are several instances of temporary "necking" or plateauing of pull force where micro-slipping is occurring in the grasp. We hypothesize that the object is leaving and entering new states of high grasp friction as the object "settles" within the grasp.

5.2.4 Test Setup and Procedure

1. Place a cylindrical artifact in the robotic hand using a wrap grasp at maximum power with the highest number of hand-object points of contact possible.

2. Pull on the pipe at a controlled rate of increasing force, recording force until gross slipping is visually confirmed between the hand and PVC pipe. Note: A future version of this test will specify force transfer rates as test parameters. These will be achievable using appropriate spring stiffnesses and pull velocity pairs.

3. Repeat the process for the desired sample size (see Appendix D for guidance)

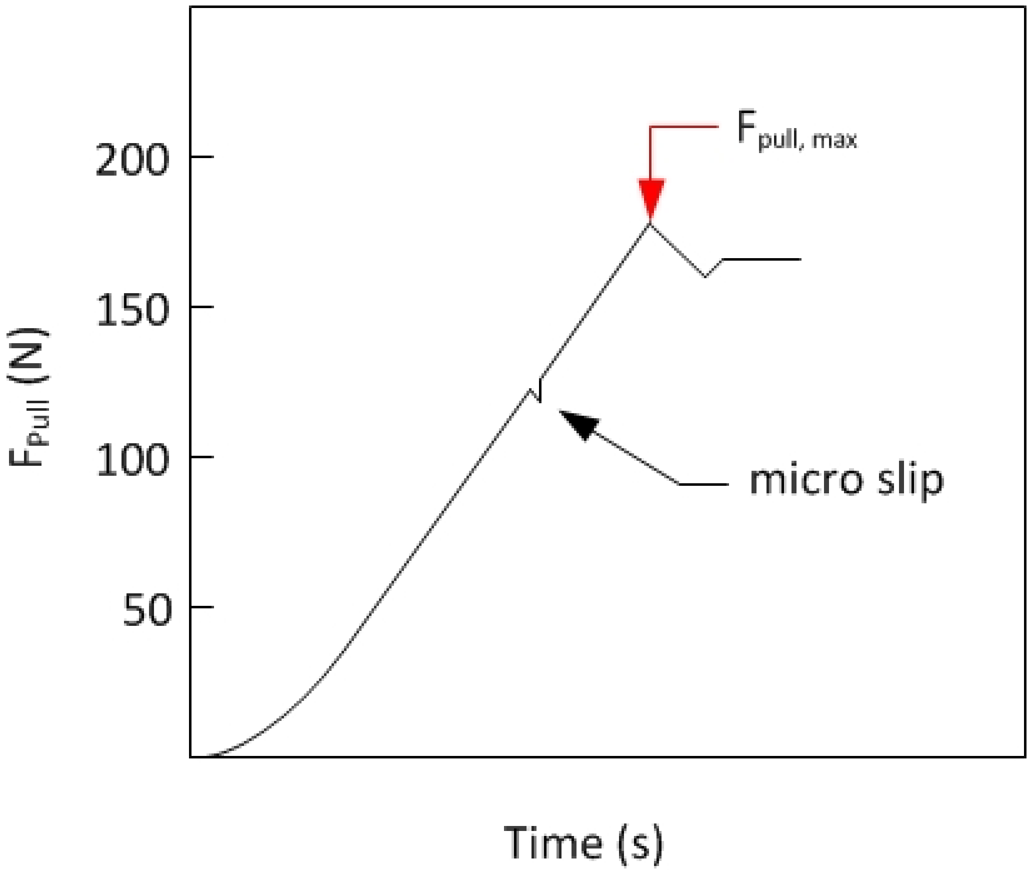

Fig. 13. Test setup for slip resistance where a standard diameter of ASTM D2665 PVC pipe is placed in a wrap grasp at maximum hand power. The pipe is then pulled at an increasing force until gross slip at $F_{pull,max}$ is observed.

4. Record force sensor data throughout the test.
5. Calculate the performance measures.
6. Repeat this test procedure over a range of standard pipe diameters that the robotic hand is capable of grasping.

5.2.5 Example Implementation

NIST performed a series of tests using the slip resistance metric and test method for Hand 1 and Hand 2. In the case of Hand 1, the resistance sensing fingertips were used since they where purchased as an option for Hand 1 and would most likely withstand the maximum forces applied during slip resistance testing. A test set-up was designed as shown in Figure 14 where a fixed robotic hand is commanded to perform a wrap grasp around standard PVC pipe. A linear drive provides a controllable pull velocity on the pipe when coupled with a cable and spring. The linear actuator is commanded to move at a constant velocity until gross slipping is visually confirmed between the hand and PVC pipe, and a peak force is shown by the load cell during data collection. This process was repeated 10 times for each robotic hand and four different cylinder diameters ranging from 2.54 cm to 10.16 cm. The measure of interest in this test is the maximum obtainable pull force for a given hand and pipe size under a full-force wrap grasp. The common trend in this test was that the pull force increased mostly linearly before reaching a peak force, and then subsequently yielded a drop in pull force (see Figure 15). Variations in the force profile could exist across different hand designs. Regardless, the maximum pull force is the metric of interest and should be acquirable regardless of the force profile. This drop after the peak force indicates a shift from static Coulomb friction to dynamic Coulomb friction. After 10 test runs were conducted across both hands, and four different pipe diameters, the relevant data was extracted and calculated. The results for both hands across all pipe diameters tested are shown in Figure 16.

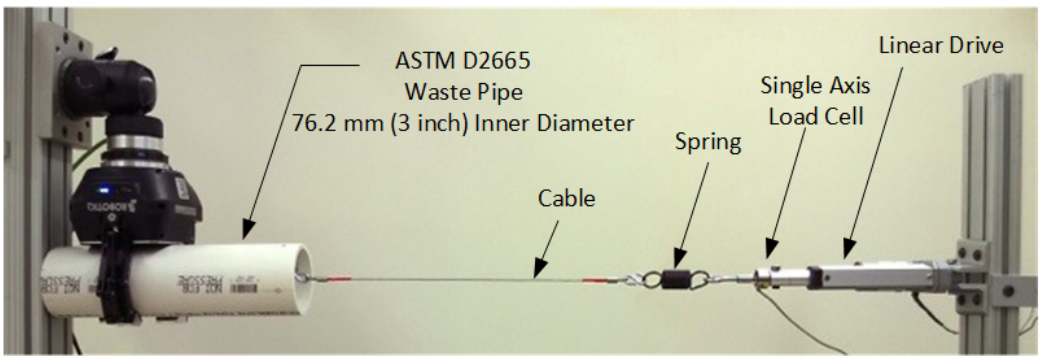

Fig. 14. Slip resistance testing on Hand 2 using a length of ASTM D2665 PVC pipe. A linear drive attached to a cable provides incremental loading on the pipe. The load rate is decreased using an in-line spring and force is recorded using a single-axis load cell.

5.2.6 Data

Data File Archive:	http://www.nist.gov/el/isd/upload/Slip-Resistance.zip
Data Files:	Hand 1/C[cylinder ID]_[test run number]
	Hand 2/C[cylinder ID]_[test run number]
Cylinder ID:	C1 = 25.4 mm (1.0 inches)
(Inside Diameter)	C2 = 50.8 mm (2.0 inches)
	C3 = 76.2 mm (3.0 inches)
	C4 = 101.6 mm (4.0 inches)
File Format:	ASCII, comma delimited
Data Values:	F_pull (one per line)
Units:	Newtons, Millimeters
Data Sample Rate:	3 kHz

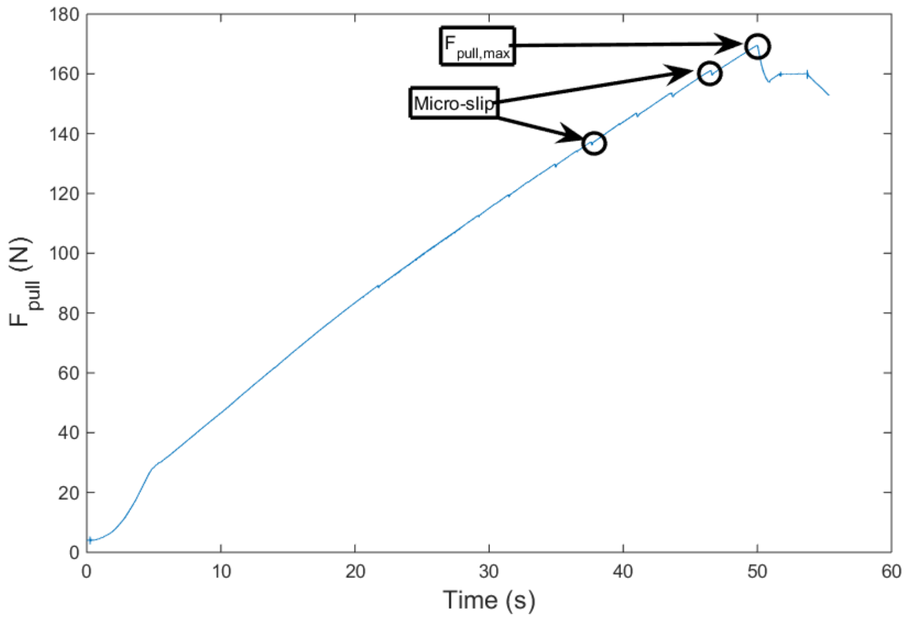

Fig. 15. Plot of the typical pull force profile as a function of time for Hand 2 under test and a 50.8 mm (2 inch) PVC pipe artifact.

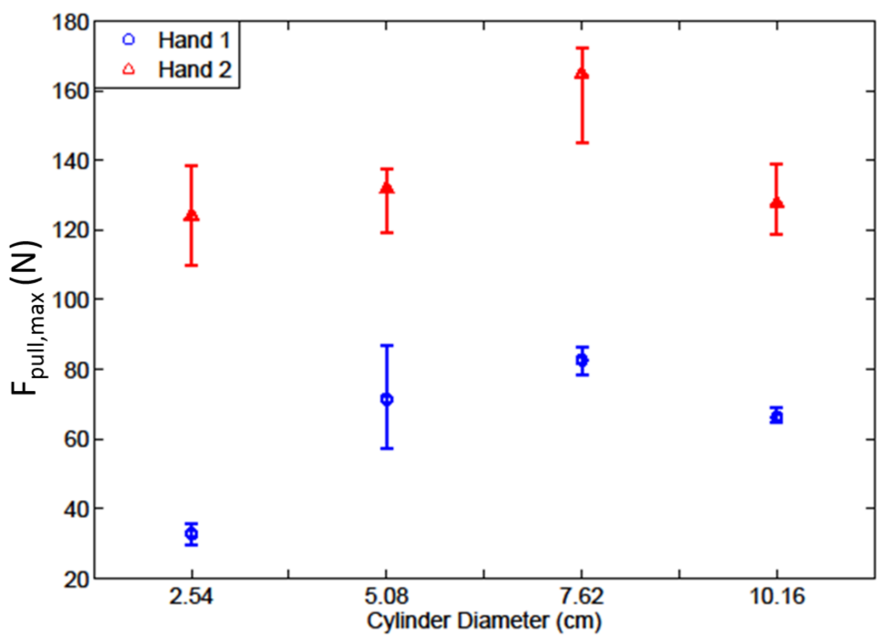

Fig. 16. The maximum pull force achieved by each hand across several PVC pipe artifacts of inner diameter ranging from 2.54 cm to 10.16 cm (1 inch to 4 inches)

6. Grasp Cycle Time

6.1 Metric

6.1.1 Definition

Grasp cycle time is a measure of the minimum time required for a robotic hand to achieve full closure from a known pre-grasp configuration and to return to the pre-grasp configuration from the grasp position. This measure will yield information regarding a hand's closing/opening speed capabilities.

6.1.2 Dependencies

Closing/Opening time is a function of the hand's: actuator capabilities, motion controllers, mechanical design, and grasp configuration.

6.2 Test Method

6.2.1 Measurement Instrument

1. Single axis load cells for one-dimensional force measurement F_i where i=1,2,...,n and n is the total number of load cells
2. Split cylinder artifacts (see Appendix C)
3. Required data acquisition hardware and software.

6.2.2 Description

Of the previously listed dependencies, only the grasp configuration and object size are assumed controllable. Two common grasp types can be chosen for investigation – pinch and wrap. The pinch grasp allows for measuring closing/opening performance associated with precision grasping, while the wrap grasp allows for measuring performance associated with power grasping. The grasp cycle of a wrap grasp is depicted in Figure 17. Artifact sizing should be chosen based on the intended application and the parts being handled. Otherwise, a reference artifact can be used to facilitate benchmarking across a variety of robotic hands.

6.2.3 Performance Measures

For each set of instantaneous force readings, add forces across all load cells since they are in-line to yield a total grasp force F_{total},

$$F_{total} = \sum_{i=1}^{n} F_i. \tag{3}$$

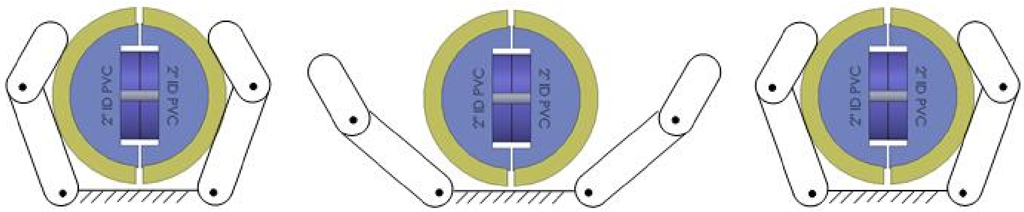

Fig. 17. Split cylinder artifact in the dominant (zero-degree) orientation relative to power grasp stages

Determine the total time between quasi-static closure to yield a grasp cycle time $T_{grasp\ cycle}$ determined by:

$$T_{grasp\ cycle} = T_{stop} - T_{start}. \tag{4}$$

T_{start} and T_{stop} are chosen as the first indication of grasp release for two subsequent grasp cycles performed (see Figure 18). Quasi-static grasp forces are chosen for evaluation as they remove impact effects and give a more accurate estimate of the time required to attain an object. For thorough experimentation, several runs should be conducted to compute $T_{grasp\ cycle}$ using two quasi-static grasp force events over two grasp cycles. Then the grasp cycle time mean and 95% confidence intervals can be computed.

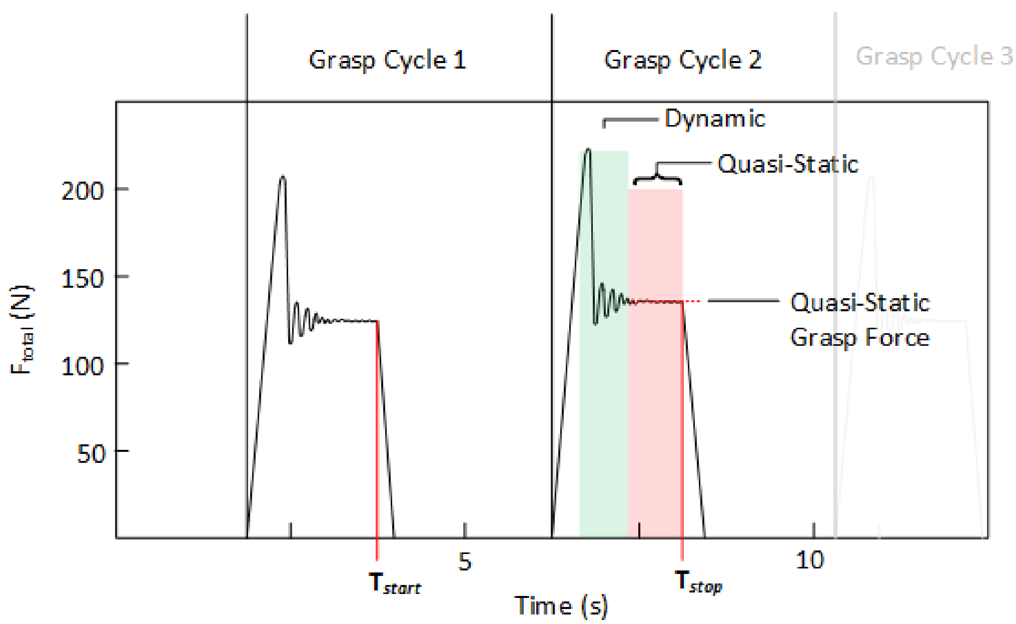

Fig. 18. Depiction of dynamic and quasi-static force regions during grasp cycles.

6.2.4 Test Setup and Procedure

1. Grasp a split cylinder test artifact in the dominant force orientation with the robotic hand under test, constraining the artifact to prevent movement when the test grasp is released.
2. Under position control, command the hand to open completely.
3. Under position control, command the hand to close completely to induce control saturation, producing the maximum force closure grasp.
4. Repeat steps 1 and 2 at maximum hand velocities for the desired sample size (see Appendix D for guidance).
5. Record force sensor data throughout the test.
6. Calculate the performance measures.

6.2.5 Example Implementation

NIST performed a series of tests using the grasp cycle time metric and test method for Hand 2. Force data was captured from two load cells while fully opening and closing the robotic hand in a power grasp around the artifact 32 times for a single orientation. The test setup is shown in Figure 19.

A data plot of F1 and F2 from the split cylinder artifact load cells throughout the 32 grasp cycles is shown in Figure 20. The F_1 time plot is used to determine the total time between quasi-static closure forces to yield grasp cycle times $T_{grasp\ cycle}$. The mean and 95% confidence intervals for $T_{grasp\ cycle}$ for Hand 2 are shown in Table 3.

	$T_{grasp\ cycle}$	
Robot	**Mean (s)**	**95% Confidence Interval (s)**
Hand 2	3.8207	[3.6432,3.9898]

Table 3. Mean and 95% confidence intervals of the internal grasp force for Hand 2

6.2.6 Data

Data File Archive:	http://www.nist.gov/el/isd/upload/Grasp-Cycle-Time.zip
Data Files:	Hand2_Grasp_Cycle_Time.csv
File Format:	ASCII, comma delimited
Data Values:	F1 and F2 (one set per line)
Units:	Newtons
Data Sample Rate:	1 kHz

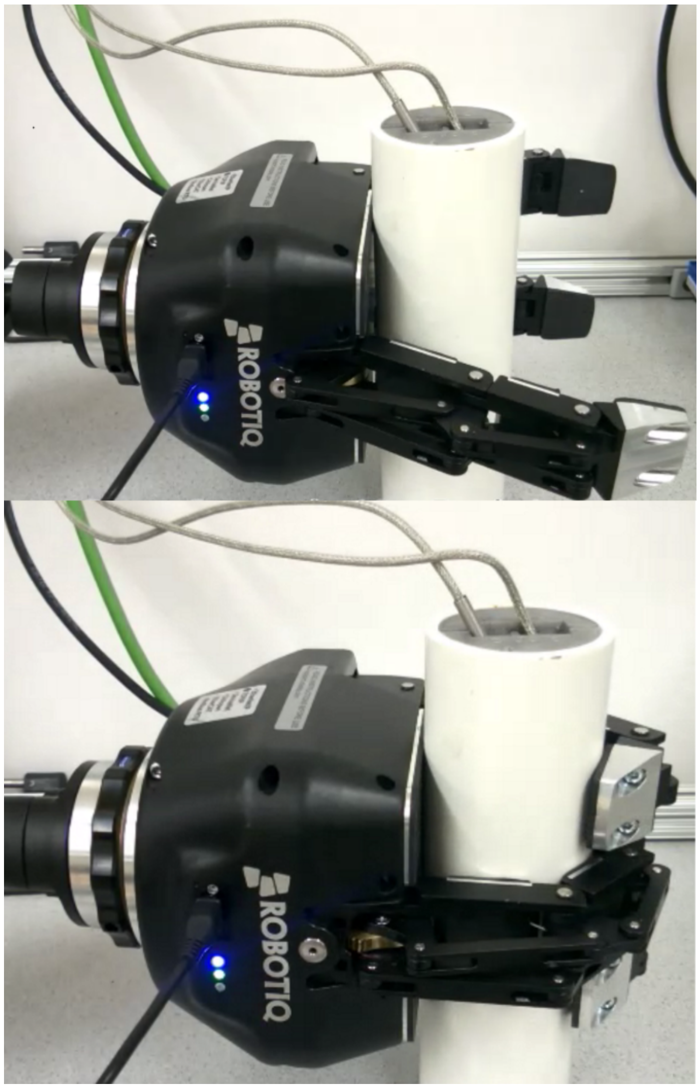

Fig. 19. 50.8 mm (2 inch) PVC split cylinder artifact with Robotic Hand 2 performing wrap grasp cycles at fully open (top) and start release (bottom) positions.

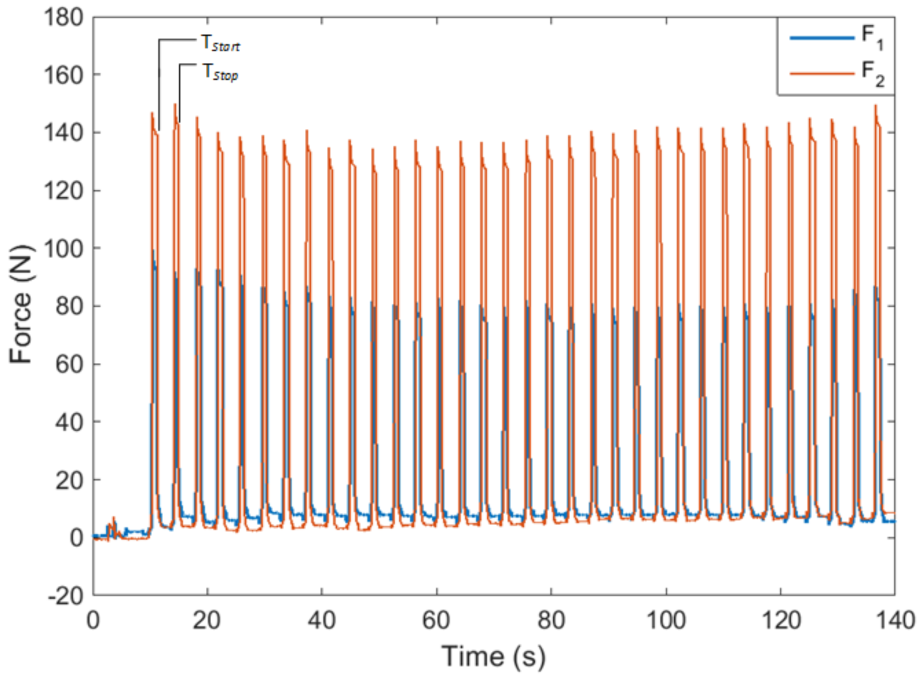

Fig. 20. Shows the load cell forces for the 50.8 mm (2 inch) PVC split cylinder artifact oriented at 0 degrees created by grasp cycles from Robotic Hand 2

7. Touch Sensitivity

7.1 Metric

7.1.1 Definition

Touch sensitivity is a kinetic measure of the smallest self-registered contact force exerted by a robotic finger on an object. The significance of this trait revolves around the hand's ability to delicately interact with minimal disturbance to the immediate environment as well as detect small force perturbations. Direct applications would include touch-based grasp planning, or part acquisition with object location or shape uncertainties.

7.1.2 Dependencies

This characteristic is a function of the hand's sensor capabilities, motion controllers, bandwidth, closing speed, finger size, and finger-object configuration.

7.2 Test Method

7.2.1 Measurement Instrument

1. Option 1: Object fixed to three-axis load cell that can measure the forces imposed on the object -or-
2. Option 2: Position tracking system to measure relative translation and rotation of an object in space during touch interaction.
3. Required data acquisition hardware and software.

7.2.2 Description

To most accurately capture the performance of a hand in this category, a dynamic test is needed. Of the touch sensitivity dependencies, only the closing speed and finger configuration are assumed controllable. The robotic finger(s) are commanded to close on an object at a specified joint velocity. An important finger-object configuration for benchmarking occurs at a specified joint velocity and at a fully-extended configuration with the finger orthogonal to the palm surface. At this configuration, the Cartesian velocity at the fingertip is maximized which will induce the highest (worst-case) impact forces upon collision. By commanding different closing speeds, a spread of behavior can be generated that will provide the user valuable insight on the trade-off between speed and touch sensitivity for any robotic hand.

7.2.3 Performance Measures

1. **Force:**
   If using a sensor capable of resolving forces in three dimensions (option 1), compute the resultant magnitude of contact forces from the load cell data, $F_{contact}$, by computing the L_2 norm of the three-dimensional contact forces as

$$Fcontact = \sqrt{\left(F_x^2 + F_y^2 + F_z^2\right)}. \tag{5}$$

   Extract the peak $F_{contact}$ for each touch test cycle over a range of hand closing speeds. After collecting these maximum forces for each closing speed, compute the mean and 95% confidence intervals to evaluate the force associated with the closing speed.

2. **Displacement:**
   If using an object position tracking system (Option 2) compute the resultant relative translation, $T_{contact}$ and rotation, $R_{contact}$

$$T_{contact} = \sqrt{\left(T_x^2 + T_y^2 + T_z^2\right)} \tag{6}$$

$$R_{contact} = \sqrt{\left(R_x^2 + R_y^2 + R_z^2\right)}. \tag{7}$$

   After collecting these displacements for each closing speed, compute the mean and 95% confidence intervals to evaluate the displacement associated with the closing speed.

7.2.4 Test Setup and Procedure

1. Place the robotic finger under test in a fully extended configuration with fingertip touch occurring on a cylinder mounted to the load cell.

2. Fully retract the finger to remove contact with the load cell (or object with position-sensing targets) and to provide sufficient offset for the finger to obtain the desired closing speed before contact.

3. While recording the load cell force data (or tracking system position data), command the hand to close at a preset joint velocity while polling the fingertip sensor for the slightest indication that contact has been established.

4. Once contact is detected by the hand, the control program automatically commands the finger to hold position.

5. Repeat the process for the desired sample size (see Appendix D for guidance)

6. Record force sensor data (or position tracking system data) throughout the test.

7. Calculate the performance measures.

7.2.5 Example Implementation

NIST performed a series of tests using the touch sensitivity metric and test method for Hand 1 and Hand 2. The test was performed with a mounted robotic hand and an external 6-axis load cell. The calibrated load cell is used as ground truth for measuring contact forces. A robotic arm was used to position the hand relative to the load cell. However, once positioned, the arm remained stationary throughout the test with its brakes engaged. The test setup is shown in Figure 21

The resultant magnitude of contact forces from the load cell data was calculated by computing the L_2 norm of the three-dimensional contact forces $F_{contact}$. This yields the overall size of the contact force exerted by the finger onto the artifact. Next, the peaks of the force data were extracted yielding the maximum impact forces for each test cycle, $F_{contact,max}$ (see Figure 22). After collecting these maximum forces for each closing speed, the mean and 95% confidence intervals were calculated to establish a most likely performance point and the uncertainty. This process was repeated ten times for six different closing velocities.

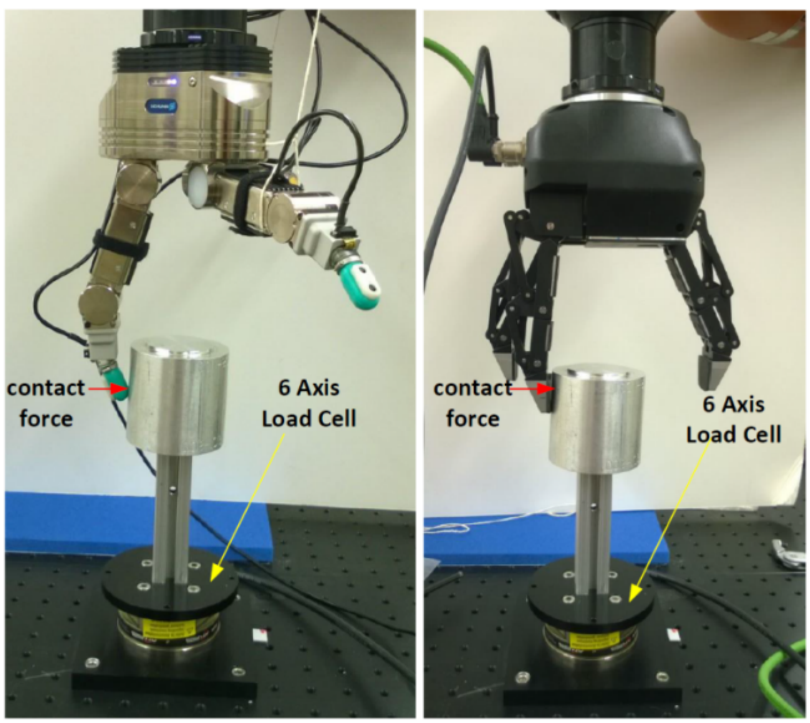

Fig. 21. Finger-artifact configuration during touch sensitivity testing; Hand 1 with impedance sensing (left) and Hand 2 (right) .

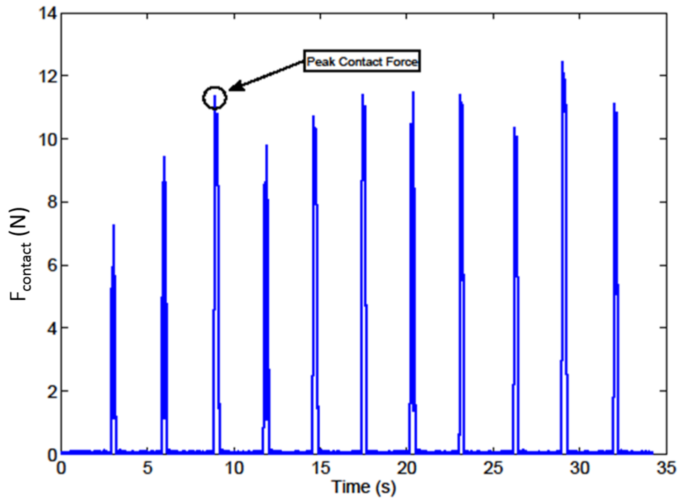

Fig. 22. Contact force profile for Hand 1, Finger 1 with resistance sensing at 20 rad/s closing speed.

After data collection and analysis across Hand 1 with impedance and resistance sensing, and Hand 2 with current sensing, the data is displayed to show not only an absolute performance, but relative performance (see Figure 23). The lower the maximum contact force, the more sensitive and reactive the finger.

7.2.6 Data

Data File Archive:	http://www.nist.gov/el/isd/upload/Touch-Sensitivity.zip
Data Files:	Hand 1 Impedance/Finger[No.]_Vel_[val]
	Hand 1 Resistance/Finger[No.]_Vel_[val]
	Hand 2/Finger[No.]_Vel_[val]
File Format:	ASCII, comma delimited
Data Values:	7 F_x, F_y, F_z (one set per line)
Units:	Newtons
Data Sample Rate:	3 kHz

8. Grasp Efficiency

8.1 Metric

8.1.1 Definition

Grasp efficiency is a measure of the hand's ability to modulate grasp force in the presence of increasing object disturbance forces, while minimizing the overall required effort. This

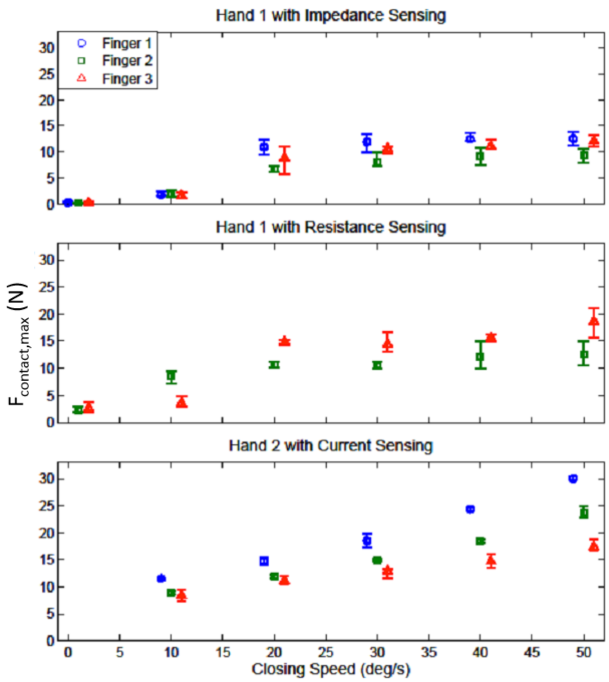

Fig. 23. Plot of maximum contact force of all robot fingers across hand 1 and hand 2 with tests for impedance, resistance, and current sensing strategies. Note that in the resistance sensing plot, Finger 1 of Hand 1 was not tested due to a faulty contact sensor.

measure will yield a hand's control and sensing capabilities regarding slip minimization and operational efficiency in grasping objects with uncertain disturbance loads.

8.1.2 Dependencies

Grasp efficiency is a function of the hand's actuator and sensing capabilities, motion controllers, mechanical design, and grasp configuration.

8.2 Test Method

8.2.1 Measurement Instrument

1. Split cylinder artifacts (see Appendix C)
2. Single axis load cell for measuring force in one dimension.
3. Required data acquisition hardware and software.
4. A mechanism for providing a controlled increasing force along the axial direction to the pipe segment.

8.2.2 Description

Of the previously listed dependencies, only the grasp configuration, object size, and object surface properties are assumed controllable. For this test, two common grasp types can be chosen for investigation – pinch and wrap. The pinch grasp allows for measuring performance associated with precision grasping, while the wrap grasp allows for measuring performance associated with power grasping. The general setup for this test is shown in Figure 24. The split cylinder artifact is used to measure the internal grasp force F_{Grasp} while an increasing force F_{Pull} is applied to the cylinder artifact in the axial direction. This test assumes that the robot hand is capable of sensing slip or friction forces, and increases F_{Grasp} as F_{Pull} increases.

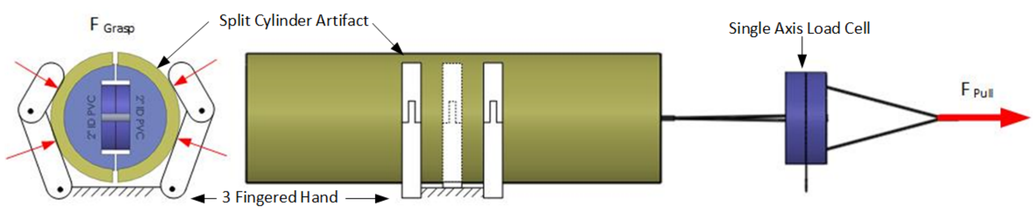

Fig. 24. Grasp efficiency setup, F_{Grasp} and F_{Pull}

In this test method, the hand is commanded to perform an initial grasp using the minimum force required to constrain the artifact $F_{Grasp,Min}$. Then, the F_{Pull} is steadily increased, ultimately approaching $F_{Pull,Max}$ as defined in the slip resistance test. F_{Grasp} and F_{Pull} are recorded throughout the test.

8.2.3 Performance Measures

For each set of instantaneous force readings, add the forces across the force sensors internal to the grasp artifact since they are in-line to yield a total grasp force F_{Grasp}, while synchronously recording F_{Pull}.

$$F_{Grasp} = \sum_{i=1}^{n} F_i. \tag{8}$$

For each test cycle (see Figure 25) compute Grasp Efficiency (E_{Grasp}) at each data point collected from the initial grasp force $F_{Grasp,Min}$ until reaching $F_{pull,max}$. Calculate grasp efficiency and compute the mean and 95 % confidence intervals to establish a most likely performance point and the uncertainty where:

$$Grasp\,Efficiency = \frac{F_{pull}}{F_{Grasp}}. \tag{9}$$

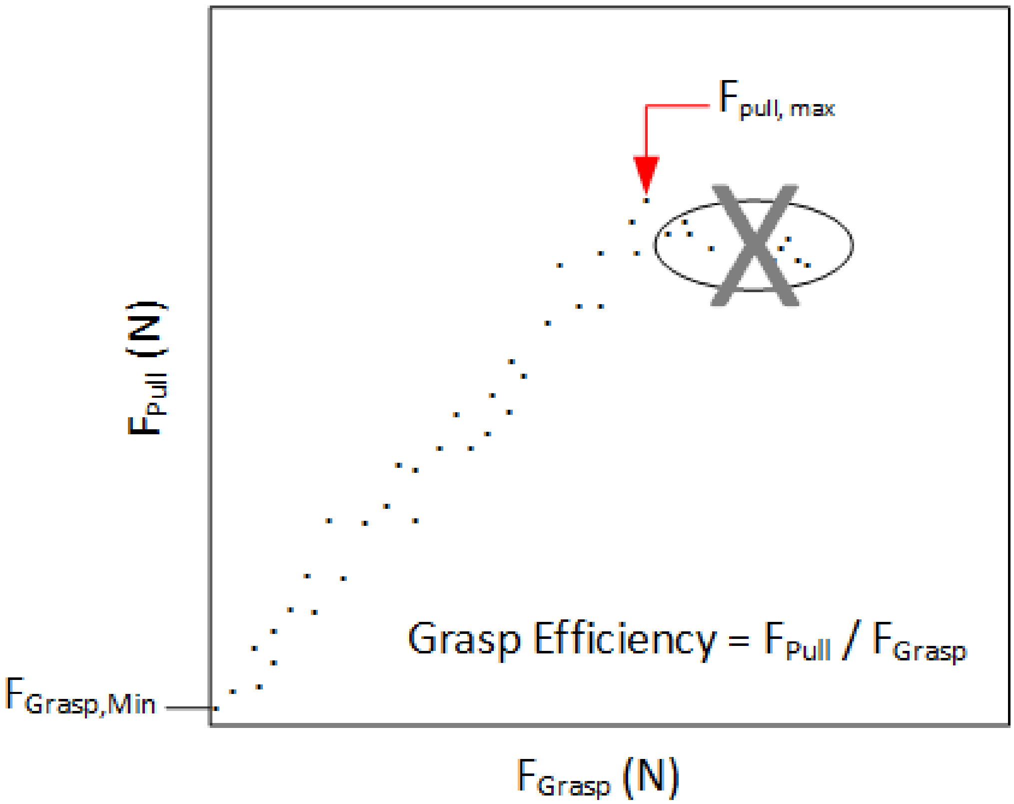

Fig. 25. Depicted grasp efficiency data, F_{Grasp} and F_{Pull}

8.2.4 Test Setup and Procedure

1. Place a cylindrical artifact in the robotic hand using a wrap grasp at minimum force to resist external forces ($F_{Grasp,Min}$) and with the highest number of hand-object points of contact possible.

2. Pull on the pipe at a controlled rate of increasing force, recording force until gross slipping is visually confirmed between the hand and the split cylinder artifact.

3. Repeat the process for the desired sample size (see Appendix D for guidance)

4. Record force sensor data throughout the test.

5. Calculate the performance measures.

6. Repeat this test procedure over a range of standard pipe diameters that the robotic hand is capable of grasping.

9. Force Calibration

9.1 Metric

9.1.1 Definitions

Force based sensor calibration is important for many state-of-the-art robotic grasping and manipulation control algorithms that use force-based control approaches. That is, to control contact forces, force sensor readings must be accurate. Moreover, force capabilities can be used for touch-based grasp planning, controlled interaction for texture discrimination, and object localization.

9.1.2 Dependencies

This characteristic is a function of the tactile sensor mechanical design, and its calibration.

9.2 Test Method

9.2.1 Measurement Instrument

1. Calibrated load cell for measuring force in three dimensions (F_x, F_y, F_z)
2. Required data acquisition hardware and software.

9.2.2 Description

This test method seeks to capture the performance of force based tactile sensors by comparing the force readings by the sensor to force data recorded simultaneously using an external load cell. Using the desired sensor-object orientation, position the sensor under test just above the force sensor and verify a zero-force reading. Press the sensor against the load cell and record both the sensor force reading and the load cell readings.

9.2.3 Performance Measures

1. **Force Magnitude:**
   Calculate the Root Mean Squared Error (RMSE) between the tactile sensor force magnitudes and those measured by the reference force sensor for all data collected. In the case of a single axis load cell, the sensor force should be applied along the load cell axis. This measure gives an indication of how competent the sensors are with predicting the correct contact force magnitude.

2. **Force Direction:**
Compute the RMSE between the force direction as measured by the tactile sensor and the external load cell. This measure gives an indication of how competent the sensors are with predicting the correct contact force directionality. This test requires the use of a three axis load cell.

3. **Maximum Force Error:**
Calculate the absolute maximum error between the contact force magnitude as measured by the hand sensor and the reference force. This measure will give an upper bound to the sensor's worst force predictions.

9.2.4 Test Setup and Procedure

1. Position the robotic finger over the measurement device as depicted in Figure 26.

2. Once in this configuration, the finger is positioned to hover over the touch point on the force sensor with zero force.

3. Under force control, the finger is then commanded to seek F_{time} a defined force profile (see example in 9.2.5).

4. Record force sensor data throughout the test to track the force profile.

5. Repeat the process for tracking the force profile according to the desired sample size (see Appendix D for guidance) per finger tested.

6. Calculate the performance measures.

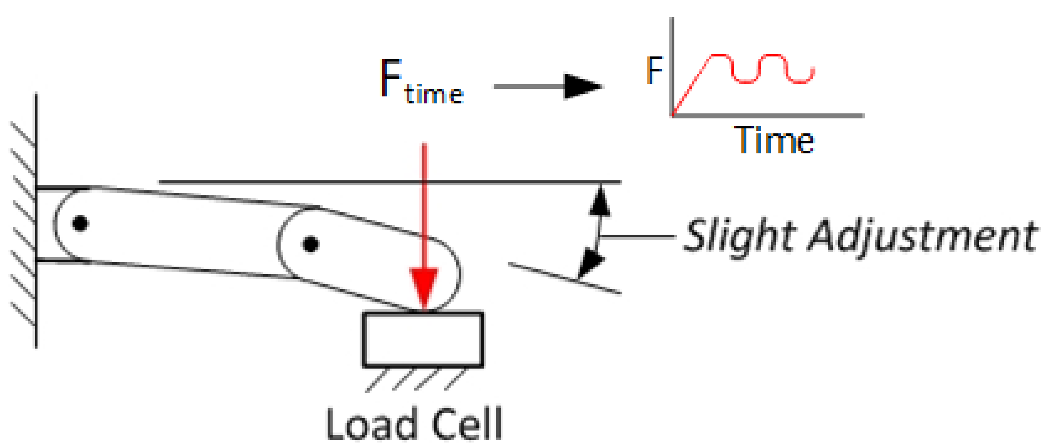

Fig. 26. Force Calibration Test Setup

9.2.5 Example Implementation

NIST performed a series of tests using the force calibration metric and test method for Hand 1. In the first test, the hand was retrofitted with resistance-based sensors at the fingertips and in the second test, the hand was fitted with impedance sensors at the fingertips. The collected data came from the finger force tracking test where each finger was commanded to seek a certain force against a flat object surface that was rigidly attached to a three-axis load cell (Figure 27). Four different force profiles were issued consisting of 1 N, $F_{finger,max}/2$ N, $F_{finger,max}$ N, and a time-varying trajectory defined as

$$||F_{d,z}|| = 5\log\left(\sin\left(\frac{\pi(t+3)}{2}\right) + \cos\left(\frac{t}{4}+\pi\right) + 3\right) + 1 \tag{10}$$

where t is time, and $F_{d,z}$ is the desired force trajectory in the world coordinate system's z-axis. Each test was conducted for a continuous 60 seconds. In the future, static calibration verification will be performed while incorporating multiple approach points to more thoroughly test larger regions of the sensor response space. Moreover, purely sinusoidal force trajectories could be issued with varying amounts of amplitude and frequency.

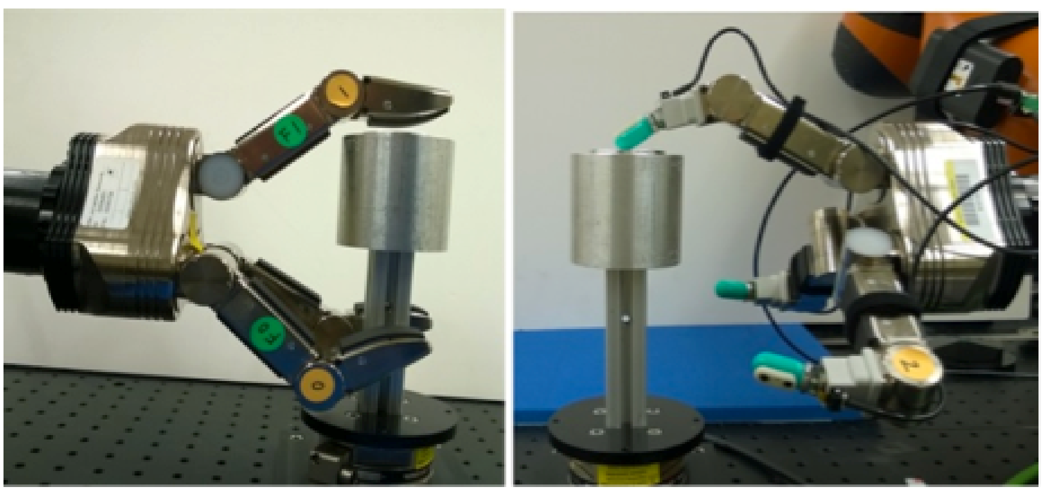

Fig. 27. Test setup for measuring performance of force calibration fidelity: Hand 1 with resistance based sensors (left) and Hand 1 with impedance sensors (right).

Three performance measures were extracted from the collected data. First, the Root Mean Squared Error (RMSE) was calculated between the sensor force magnitudes and those measured by the reference force sensor for all data collected. Next, the RMSE was calculated between the force direction as measured by each sensor and the reference load cell. Lastly, the maximum force error is calculated between the desired contact force magnitude and the measured contact force magnitude. Combined results are shown in Table 4.

Robotic Hand	$\|\|F_d\|\|$ N	RMSE (N) $\|\|F_L\|\| - \|\|F_S\|\|$	RMSE $\hat{F}_L - \hat{F}_S$	Maximum Force Error (N)
Hand 1 (Impedence Sensing)	1	1.054	[0.412; 0.529; 0.285]	3.004
	$\frac{F_{finger,max}}{2}$	2.855	[0.254; 0.248; 0.118]	7.108
	$F_{finger,max}$	2.170	[0.087; 0.154; 0.038]	9.084
	Eq. 1	2.711	[0.201; 0.257; 0.099]	7.191
Hand 1 (Resistance Sensing)	1	2.586	[0.218; 0.280; 0.815]	6.380
	$\frac{F_{finger,max}}{2}$	4.825	[0.075; 0.427; 0.144]	13.386
	$F_{finger,max}$	4.939	[0.062; 0.336; 0.101]	16.398
	Eq. 1	5.411	[0.093; 0.359; 0.158]	13.003

Table 4. Various force calibration performance errors for Hand 1 under both impedance and resistance-based contact sensing

9.2.6 Data

Data File Archive:	http://www.nist.gov/el/isd/upload/Finger-Force-Tracking.zip
Data Files:	Hand 1 Impedance/Set Point/Finger[No_[File Type.]_ [Magnitude]N
	Hand 1 Impedance/Time Varying/Finger[No.]_[File Type.]
	Hand 1 Resistance/Set Point/Finger[No.]_[File Type]_ [Magnitude]N
	Hand 1 Resistance/Time Varying/Finger[No.]_[File Type]
	Hand 2 /Set Point/Finger[No.]_[File Type]_[Magnitude]N
File Type:	Loadcell - reference load cell
	Impedance - impedance contact sensing
	Resistance - resistance contact sensing
File Format:	ASCII, comma delimited
Data Values:	F_x, F_y, F_z (one set per line)
Units:	Newtons
Data Sample Rate:	3 kHz

10. Finger Force Tracking

10.1 Metric

10.1.1 Definition

Finger force tracking is a kinetic measure regarding the finger's ability to impose desired contact forces on its environment. This capability is particularly important for many state-of-the-art robotic grasping and manipulation control algorithms that use force-based control approaches. Moreover, this capability can be used for touch-based grasp planning, controlled interaction for texture discrimination, and object localization.

10.1.2 Dependencies

This characteristic is a function of the hand's actuator capabilities, tactile sensor calibration, motion and force controllers, control and sensing bandwidth, mechanical design, finger-artifact configuration, and the parameters of the selected contact force trajectory.

10.2 Test Method

10.2.1 Measurement Instrument

1. Calibrated load cell for measuring force in three dimensions (F_x, F_y, F_z)
2. Required data acquisition hardware and software.

10.2.2 Description

This test method seeks to capture the force tracking performance of an individual finger of a robotic hand. Of the finger force tracking dependencies, only the finger-artifact configuration and the parameters of the desired contact force profile are assumed controllable. The test begins by commanding the finger under test to track a desired force profile by contacting an artifact attached to a reference load cell. The parameters of this desired force profile can vary in contact force directionality as well as magnitude. In addition, the finger-artifact configuration can also be varied to test performance for different contact scenarios. During the test, the desired force profile $(F_d \in \mathbb{R}^{3x1})$, the contact forces measured by the finger sensor $(F_S \in \mathbb{R}^{3x1})$, and the contact forces measured by the load cell $(F_L \in \mathbb{R}^{3x1})$ are all recorded for extracting performance measures. This test assesses the total force tracking performance, and the controller force tracking performance. In the former, the desired profile data is compared to the reference force sensor data to establish real-world force tracking performance. In the latter, the desired profile data is compared to the hand sensor data to establish only the controller force tracking performance. For both considerations, the following performance measures are extracted.

10.2.3 Performance Measures

1. **Force Magnitude:**
   Calculate the Root Mean Squared Error (RMSE) between the desired force magnitudes ($||F_d|| \in \mathbb{R}$) and those measured by either the reference force sensor ($||F_L|| \in \mathbb{R}$) or hand sensor ($||F_S|| \in \mathbb{R}$) for all data collected. In the case of a single axis load cell, the sensor force should be applied along the load cell axis.

2. **Force Direction:**
   Compute the RMSE between the desired force direction ($||F_d|| \in \mathbb{R}^{3x1}$) and the direction as measured by the external load cell ($||F_L|| \in \mathbb{R}^{3x1}$) or hand sensor ($||F_S|| \in \mathbb{R}^{3x1}$). This measure has three dimensions (one for each axis) and therefore requires the use of a three-axis load cell. Note: Only performed on robotic hands with sufficient degrees of freedom.

3. **Force Peak Overshoot:**
   Calculate the peak overshoot ($||F_{peak}|| \in \mathbb{R}$) between the desired contact force magnitude and the contact force magnitude as measured by the reference sensor or hand sensor. This measure will give an upper bound to the finger's control response.

10.2.4 Test Setup and Procedure

1. Position the robotic finger in a fully-extended position as depicted in Figure 28.

2. Once in this configuration, the finger is positioned to hover over the touch point on the force sensor with zero force.

3. Under force control, the finger is then commanded to seek a defined force profile (see example in 10.2.5).

4. Record force sensor data throughout the test to track the force profile.

5. Repeat the process for tracking the force profile according to the desired sample size (see Appendix D for guidance) per finger tested.

6. Calculate the performance measures.

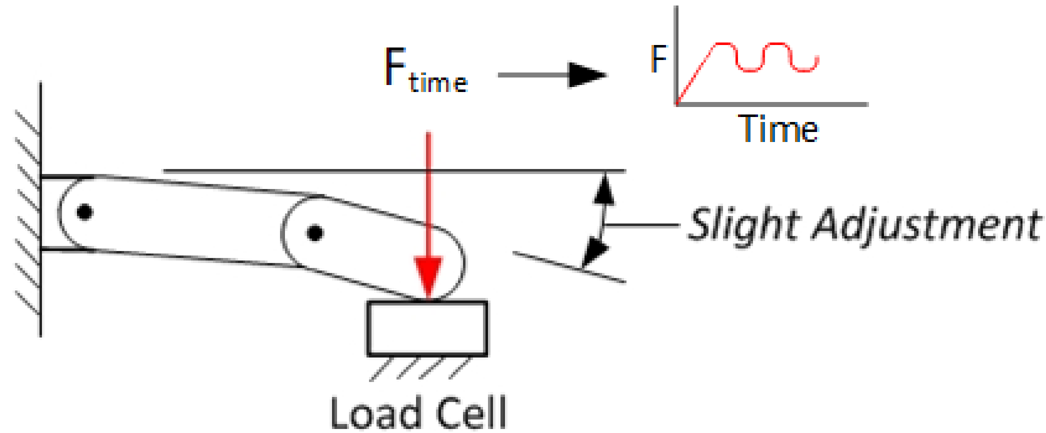

Fig. 28. Force Calibration Test Setup

10.2.5 Example Implementation

NIST performed a series of tests using the force calibration metric and test method with Hand 1 and Hand 2. Hand 1 was first retrofitted with impedance sensors at the fingertips and then with resistance based sensors at the fingertips. Hand 2 uses motor currents to sense force per finger. To extract force tracking performance, each finger for each robotic hand is commanded to exert a specified force profile onto an artifact mounted to an external force sensor (in this case, 6-axis load cell) as shown in Figure 29. In the case of this experimentation, four distinct forces profile magnitudes were prescribed for testing. Three were fixed-force profiles of 1N, $||F_{finger,max}||/2$ N, and $||F_{finger,max}||$ N where $F_{finger,max}$ is the maximum finger force capability as determined in the previous test for finger strength. The final force profile was time-varying in nature with two frequencies and varying amplitudes defined by

$$||F_d|| = 5\log\left(\sin\left(\frac{\pi\,(t+3)}{2}\right) + \cos\left(\frac{t}{4} + \pi\right) + 3\right) + 1 \tag{11}$$

This equation is purposefully scaled in magnitude to remain within the maximum force strength capabilities of the robotic hand under test. The direction of all force profile magnitudes was vertically downward into the artifact mounted to the force sensor (see Figure 29). Different force profiles will be added and tested in the future. Because of the current control limitations of Hand 2, only the fixed-force step functions were applied to test the hand's ability to achieve a force.

The test is performed on two hand configurations; Hand 1, a robotic hand platform retrofitted with resistance based fingertip sensors, and Hand 1, the same robotic hand platform retrofitted with impedance based fingertip sensors. The test begins by positioning either Hand 1 such that the palm is parallel to the vertical axis of the artifact. Next, the finger under test was placed in a configuration of maximum manipulability with the fingertip parallel to and

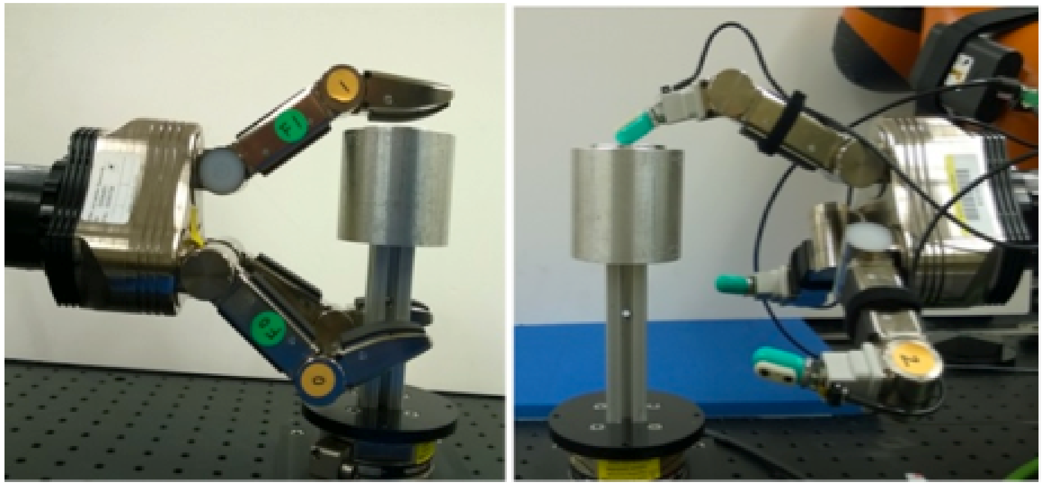

Fig. 29. Test setup for finger force tracking: Hand 1 with resistance based fingertip sensors (left), Hand 1 with impedance based fingertip sensors (right).

offset by approximately 1 cm from the artifact surface. For Hand 1, the maximum manipulability finger pose resulted in joint angles of -45 degrees for the first joint, and 45 degrees for the second joint. Since Hand 2 is underactuated and possesses only one degree of freedom per finger, the specification of joint angles for maximum manipulability is not relevant. Different finger-artifact configurations will be added and tested in the future.

Each finger was then commanded to track the desired force profile, and the contact forces were measured using the external force sensor. Since Hand 1 exhibited continuous force tracking control capability, it was tasked with tracking the desired profile for 60 seconds. Since Hand 2 used a simpler stop-and-hold strategy upon achieving the desired force, it was tasked to cyclically achieve the desired force by lifting off and making contact again, a process that was repeated ten times for each finger. For both hands, the force profile was used to generate a mean performance and its uncertainty measures.

The three performance measures were extracted from the collected data that concern the total force tracking performance (controller performance will be added in the future). First, the Root Mean Squared Error (RMSE) was calculated between the desired force magnitudes and those measured by the reference force sensor for all data collected (see Figure 30 for example visualization of force controller results). This measure gives an indication of how well the fingers impart desired contact force magnitudes. Second, the RMSE between the desired force direction and measured contact force direction is calculated. This measure has three dimensions (one for each axis). Lastly, peak overshoot, a measure often used to indicate controller performance, is calculated between the desired contact force magnitude and the measured contact force magnitude. Results for Hand 1 and Hand 2 are shown in Table 5. The lower the RMSE reported values, the closer the hand was to imparting the pre-defined force profile. The lower the peak overshoot, the lower the maximum error between the desired and imparted forces. Hand 2 is under-actuated and therefore does have any reportable measures for RMSE for the force control directions.

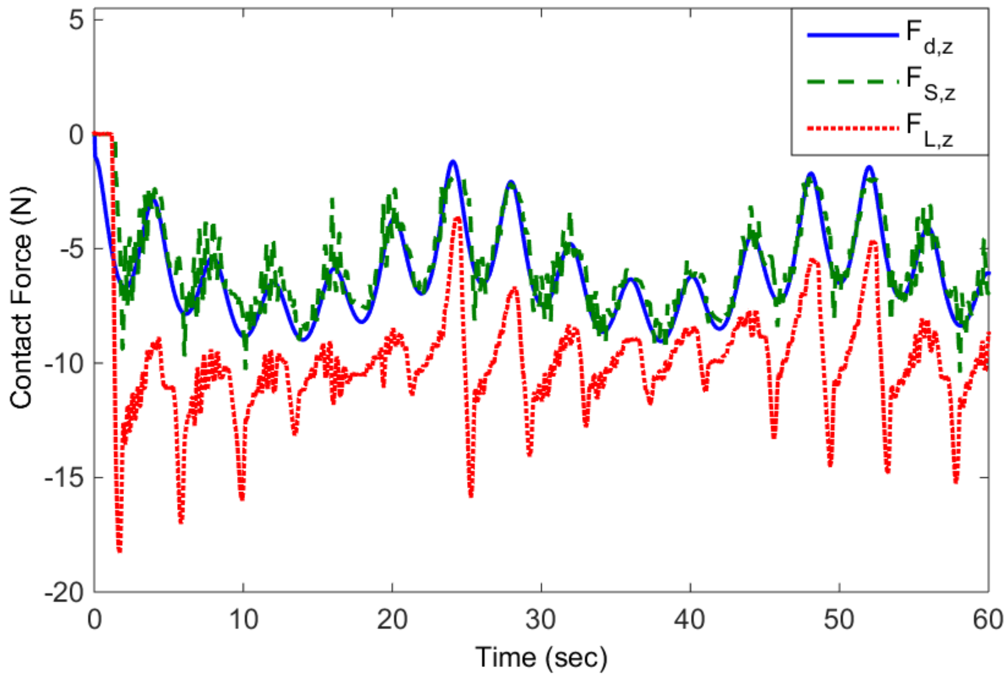

Fig. 30. The desired force profile ($F_{dffi,Z}$), the contact force as sensed by the onboard sensor ($F_{S,Z}$), and the contact force as sensed by an external load cell ($F_{L,Z}$) for Hand 1, finger 2 with resistance sensing.

10.2.6 Data

Data File Archive:	http://www.nist.gov/el/isd/upload/Finger-Force-Tracking.zip
Data Files:	Hand 1 Impedance/Set Point/Finger[No_[File Type.]_ [Magnitude]N
	Hand 1 Impedance/Time Varying/Finger[No.]_[File Type.]
	Hand 1 Resistance/Set Point/Finger[No.]_[File Type]_ [Magnitude]N
	Hand 1 Resistance/Time Varying/Finger[No.]_[File Type]
	Hand 2/Set Point/Finger[No.]_[File Type]_[Magnitude]N
File Type:	Loadcell - reference load cell
	Impedance - impedance contact sensing
	Resistance - resistance contact sensing
File Format:	ASCII, comma delimited
Data Values:	F_x, F_y, F_z (one set per line)
Units:	Newtons
Data Sample Rate:	3 kHz

Robotic Hand	$\|\|F_d\|\|$ N	RMSE (N) $\|\|F_d\|\| - \|\|F_L\|\|$	RMSE $\hat{F}_d - \hat{F}_L$	Force Peak Overshoot (N)
Hand 1 (Impedence Sensing)	1	0.567	[0.124; 0.428; 0.323]	1.046
	$\frac{F_{finger,max}}{2}$	2.182	[0.020; 0.225; 0.102]	4.972
	$F_{finger,max}$	1.773	[0.015; 0.134; 0.021]	5.159
	Eq. 1	2.092	[0.024; 0.204; 0.082]	5.160
Hand 1 (Resistance Sensing)	1	2.121	[0.218; 0.285; 0.483]	6.382
	$\frac{F_{finger,max}}{2}$	4.577	[0.075; 0.398; 0.178]	12.028
	$F_{finger,max}$	4.032	[0.062; 0.283; 0.133]	16.746
	Eq. 1	5.013	[0.093; 0.330; 0.223]	14.223
Hand 2 (Current Sensing)	1	N/A	N/A	N/A
	$\frac{F_{finger,max}}{2}$	1.226	N/A	2.864
	$F_{finger,max}$	5.129	N/A	-3.012*
	Eq. 1	N/A	N/A	N/A

Table 5. Various force tracking performance errors for the three force-controlled hand layouts

11. In-Hand Manipulation

11.1 Metric

11.1.1 Definition

In-hand manipulation is a kinematic measure of how well a robotic hand can control the pose of an object. The pose of an object is described in Cartesian coordinates, and the manipulation efficacy is captured in terms of control error between the desired object Cartesian pose and the measured object Cartesian pose over a time-varying trajectory. This capability is arguably one of the most difficult to achieve and measure, but is paramount to achieving dexterous robotic systems.

11.1.2 Dependencies

In-hand manipulation is an apex function for a robotic hand, and therefore depends on everything ranging from its mechatronic design and basic components to its control software. Performance is also substantially dependent on the object's properties: friction coefficient, mass, mass distribution, geometric dimensions, and morphology. Performance also depends on finger-object contact configuration, and number of fingers as well.

11.2 Test Method

11.2.1 Measurement Instrument

1. Position tracking system to measure relative translation and rotation of an object in space during touch interaction.
2. Required data acquisition hardware and software.
3. Objects retrofitted with sensors or markers to measure the object's Cartesian pose during manipulation with the position tracking system.

11.2.2 Description

Of the in-hand manipulation dependencies, only the object will be taken as a controlled test variable. It will be up to the user to place the fingers appropriately on the object that maximizes performance. Once appropriate contact has been established by an object and a robotic hand, an object-fixed coordinate system should be known to both the robotic hand and the reference measurement system with the respective transformations. From the object's initially grasped pose, $r_c\left(t_0\right) \in \mathbb{R}^{6x1}$, t_0 is the time at initial grasp acquisition, the hand should individually manipulate the object along as many independent Cartesian axes as possible (up to six) along a desired Cartesian trajectory, r_{cd} (t)$\in \mathbb{R}^{6x1}$,$r_{cd} = [x, y, z, \gamma, \beta, \alpha]$, where x,y,z are translations and γ, β, α are rotations about the X, Y, and Z axes. Along each viable axis, the object should be moved both positively and negatively from the initial condition (starting point) on that axis. The desired magnitude and rate of travel from r_c (t_0) should be recorded. A simple method for doing so is to define the desired Cartesian trajectory as $r_{cd,i}\ (t) = A\sin(2\pi f t) + r_{c,i}\ (t_0)$ for i=1,...,6. In this case, A is the motion magnitude, and f is the number of motion cycles per second. The total manipulation error, $e_{total} = r_{cd} - r_c$, should be recorded over time during a manipulation test.

11.2.3 Performance Measures

The main performance measure should be the Root Mean Squared Error of e_{total}, $RMSE_{e,total}$. $RMSE_{e,total}$ is calculated for each set of manipulation tests. For thorough experimentation, several runs should be conducted for a manipulation test, and the mean and standard deviation of $RMSE_{e,total}$ can be calculated to capture a more accurate representation of performance.

11.2.4 Test Setup and Procedure

1. Register a six degree of freedom position measurement device with the base coordinate system of the robotic hand (typically the palm).

2. Attach corresponding markers or attachments to objects under manipulation (if required by measurement device).

3. Acquire an initial grasp on the object with the robotic hand.

4. Command the robotic hand to change the pose of the object along a pre-defined trajectory.

5. Record the commanded trajectory, and the motion trajectory as measured by both the hand (if available) and reference measurement device.

6. Repeat this process for a variety of objects and sinusoidal amplitudes and frequencies.

7. Calculate the performance measures.

11.2.5 Example Implementation

NIST performed a series of tests using the in-hand manipulation metric and test method for Hand 1, a three-fingered, 7 degree-of-actuation robotic hand retrofitted with bio-inspired impedance based tactile sensors (Figure 31). Also shown in this figure are three geometrically primitive artifacts – sphere, cuboid, and cylinder. The sphere has a diameter of

120 mm and mass of 286 g, the cuboid has dimensions of 90 mm by 90 mm by 75 mm and a mass of 178 g, and the cylinder has a diameter of 90 mm, a height of 75 mm, and a mass of 143 g. The artifacts are retrofitted with reflective markers for position tracking using a motion capture system (MOCAP). The time-variant desired translation and rotation trajectories were defined as follows:

1. $r_{cd,z}$=-0.0075 sin(t) + 0.1425 (m)
2. $r_{cd,\alpha} = -\frac{\pi}{25}\sin(1.25t)(rad)$
3. $r_{cd,\beta} = -\frac{\pi}{25}\sin(0.75t)(rad)$

For these objects, these three pose axes were deemed controllable by this hand, and therefore, $r_{cd,x}$, $r_{cd,y}$, and $r_{cd,\alpha}$ were left equal to their respective initial conditions.

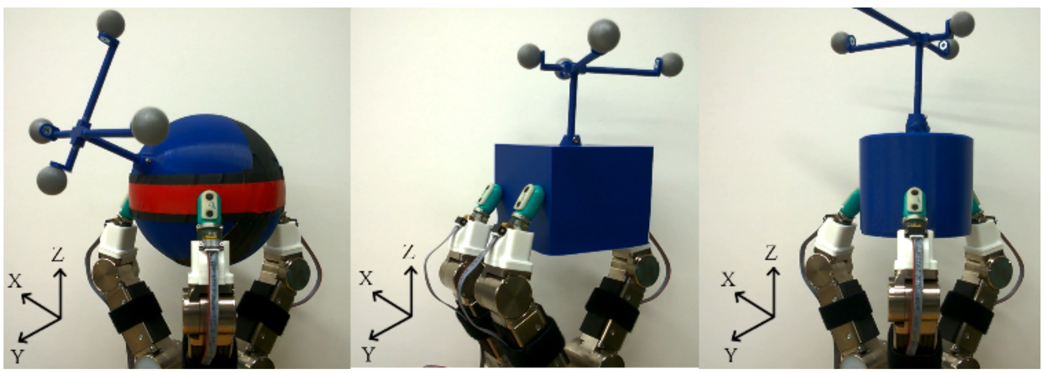

Fig. 31. Robotic hand holding a sphere (left), a cuboid (center), and a cylinder (right) with reflective markers attached for object motion tracking.

The desired object trajectory can be deconstructed in terms of manipulation amplitude and frequency as shown in Table 6.

r_{cd} component	Amplitude, A	Frequency, f (Hz)
$r_{cd,x}$	N/A	N/A
$r_{cd,y}$	N/A	N/A
$r_{cd,z}$	7.5 (mm)	0.16
$r_{cd,\gamma}$	7.2 (deg)	0.20
$r_{cd,\beta}$	7.2 (deg)	0.12
$r_{cd,\alpha}$	N/A	N/A

Table 6. Motion magnitude and motion cycles per second across independent axes

Given these trajectory parameters, the following manipulation performance was captured in Table 7. The orientation error remained relatively low. The translation performance was

Object	$RMSE_{e,total}$ (mm)	$RMSE_{e,total}$ (deg)
Sphere	[19.61,6.05,1.89]	[0.79,0.57,1.20]
Cuboid	[8.93,5.15,2.55]	[1.21,0.58,0.41]
Cylinder	[12.57,6.85,2.57]	[0.76,0.62,1.48]

Table 7. Total manipulation performance for object translation and object orientation

most accurate in the Z-axis across all objects. Substantial translation error accrued in the X and Y axes.

Notes:

The desired trajectories were concatenated for a single manipulation operation. Retrospectively, a single manipulation test should consist of the hand manipulating the object along a single, independent axis only.

12. Object Pose Estimation

12.1 Metric

12.1.1 Definition

Object pose estimation is a kinematic measure of how well a robotic hand can estimate the pose of an object. The pose of an object is described in Cartesian coordinates, and the estimation fidelity will be captured in terms of the error between the hand-estimated Cartesian pose versus the reference-measured Cartesian pose. Object pose estimation is useful feedback for in-hand manipulation control and hand-arm coordination and control, particularly since visual occlusions for an external vision system typically occur when grasping an object.

12.1.2 Dependencies

System dependencies for object pose estimation can vary considerably based on strategy. Strategies can fall into one of two main categories – contact or non-contact. If requiring object contact, then pose estimation capabilities will likely involve proprioceptive and cutaneous sensory systems as well as the driving algorithm for making the estimations. In this case, estimation performance will depend on these underlying sensors and the overarching estimation algorithm. For the non-contact strategy, a vision strategy is likely used that will depend on the vision sensor and supporting algorithms. Overall performance is likely to also depend on the object's properties as well including morphology, orientation, and optical traits.

12.2 Test Method

12.2.1 Measurement Instrument

1. Position tracking system to measure relative translation and rotation of an object in space during touch interaction.

2. Required data acquisition hardware and software.

3. Objects retrofitted with sensors or markers to measure the object's Cartesian pose during manipulation with the position tracking system.

12.2.2 Description

Of the previously listed dependencies, only the object will be taken as a controlled test variable. It will be up to the user to place the object appropriately within the hand and establish an object-fixed coordinate system and a ground coordinate system. The object-fixed coordinate system should be known to both the robotic hand and the reference position tracking system with the relevant transformations. The object should be moved through a variety of poses with respect to the hand, while object poses are estimated by the hand and "ground-truth" poses are measured by the reference position tracking system.

12.2.3 Performance Measures

The main performance measure should be the Root Mean Squared Error of $e_{estimation}$, $RMSE_{e,estimation}$, where $e_{estimation}$= $r_{c,estimation}$- $r_c \in \mathbb{R}^{6x1}$. Furthermore, r_c is the pose of the object as measured by the reference position tracking system, and is defined as, $r_c = [x, y, z, \gamma, \beta, \alpha]$, where x,y,z are translations and γ, β, α are rotations about the X, Y, and Z axes. Finally, $r_{c,estimation}$ is the pose of the object as estimated by the robotic hand. $RMSE_{e,estimation}$ is calculated separately for a variety of parts. For thorough experimentation, several runs should be conducted per object, and the mean and 95% confidence interval of $RMSE_{e,estimation}$ can be calculated to capture a more accurate representation of performance.

12.2.4 Test Setup and Procedure

1. Register a six degree of freedom position measurement device with the base coordinate system of the robotic hand (typically the palm).

2. Attach corresponding markers or attachments to objects under manipulation (if required by measurement device).

3. Acquire an initial grasp on the object with the robotic hand.

4. Command the robotic hand to change the pose of the object along a pre-defined trajectory.

5. Record the commanded trajectory, and the motion trajectory as measured by both the hand and reference measurement device.

6. Repeat this process for a variety of objects and sinusoidal amplitudes and frequencies.

7. Calculate the performance measures.

12.2.5 Example Implementation

NIST performed a series of tests using the in-hand manipulation metric and test method for Hand 1, a three-fingered, 7 degree-of-actuation robotic hand retrofitted with bio-inspired tactile sensors (Figure 31). Also shown in this figure are three geometrically primitive artifacts – sphere, cuboid, and cylinder. The sphere has a diameter of 120 mm and mass of 286 g, the cuboid has dimensions of 90 mm by 90 mm by 75 mm and a mass of 178 g, and the cylinder has a diameter of 90 mm, a height of 75 mm, and a mass of 143 g. The artifacts are retrofitted with reflective markers for position tracking using a motion capture system (MOCAP). The time-variant desired translation and rotation trajectories were defined as follows:

1. $r_{cd,z}$=-0.0075 sin(t) + 0.1425 (m)

2. $r_{cd,\alpha} = -\frac{\pi}{25}\sin(1.25t)(rad)$

3. $r_{cd,\beta} = -\frac{\pi}{25}\sin(0.75t)(rad)$

This implementation is a contact-based object pose estimation solution, and therefore the hand was tasked with manipulating the object along the above-defined trajectories in order to induce object motion and estimate the object's pose. See the In-hand Manipulation test method.

Given these trajectories, object pose estimation performance was captured in Table 8. Interestingly, the orientation error remained relatively low. The translation performance was most accurate in the Z-axis across all objects. Substantial translation error accrued in the X and Y axes.

Object	$RMSE_{e,estimation}$ (mm)	$RMSE_{e,estimation}$ (deg)
Sphere	[18.00,4.57,2.34]	[2.98,3.37,3.23]
Cuboid	[8.45, 6.82,2.76]	[2.05,1.81,2.87]
Cylinder	[11.88,5.66,2.50]	[1.97,1.29,3.07]

Table 8. Total manipulation performance for object translation and object orientation

Notes:
It is observed that estimation errors are largely due to finger-object slipping that was not detectable or incorporated by the robotic hand.

Acknowledgments

The authors would like to thank the metrics working group formed under the Institute of Electrical and Electronic Engineers (IEEE) Robotics and Automation Society Robotic Hand Grasping and Manipulation (RHGM) Technical Committee for their constructive comments that improved the overall quality, thoroughness, and usefulness of this publication.

Appendix A: Background on Grasp Performance Measures

A.1 Quantitative Grasp Measures

The physical results of grasping are reported using both qualitative and quantitative data. Qualitative data is a categorical measurement expressed by means of a natural language description where quantitative data is a numerical measurement. Qualitative measures expressing the ability to grasp an object are commonplace and typically use pass/fail indicators along with a description of how well a grasp was performed on a given test (e.g., grasp A is not as stable as grasp B, the object was ejected from the grasp). Another aspect of performance testing is functional vs. non-functional tests. Functional tests evaluate a robotic hand and overall robotic system's ability to perform the grasp required to accomplish a specific task (e.g., holding and operating tools, grasping and turning valves, and operating a door knob after unlocking it with a key) [7–9], while non-functional tests would be designed to measure more general properties of a robot hand outside the scope of an integrated robotic system. Both qualitative and quantitative measures can be used to express the results of functional and non-functional tests. Qualitative measures are easily found in robotic grasping research literature, however, examples of applying quantitative measures to evaluate grasp performance are sparse.

A.2 Volumetric

In [**?**], the authors propose a benchmark to measure the kinematic ability of a robotic hand to grasp objects. In particular, cylindrical objects of increasing diameter (40, 50, 55, 60, 63, 75, 90, 110, 115, and 120 mm) were used under both pinch grasps and enveloping grasps. In the case of a pinch grasp, the outermost point of the object circumference was placed a distance of L from the palm and in the case of an enveloping grasp, the object was placed against the palm. Also noted during grasps were the cases where a pinch grasp resulted in the hand pulling the artifact towards the palm resulting in a transition to a final enveloping grasp equilibrium. A performance metric was defined as follows:

$$Q_{grasp} = \frac{\frac{\pi}{2}\delta D_{obj}}{2L+2Lo}, \tag{12}$$

where, δD_{obj} is the difference between the diameter of the largest and smallest graspable object, $L = L_1 + L_2$ is the length of one finger and $2L_0$ is the palm width of the hand (Figure 32).

A.3 Internal Force

Odhner et al. implemented a test apparatus to test the power grasp capabilities of the iRobot-Harvard-Yale (iHY) Hand, a compliant under-articulated hand that used tendons to actuate finger motion [2]. The apparatus was constructed of a split cylinder and a load cell

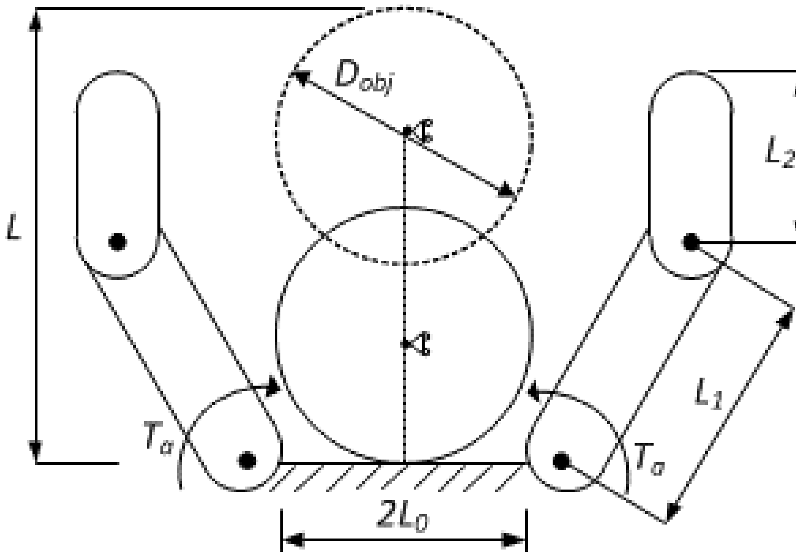

Fig. 32. Reproduced from [1], initial positions of a freely moving cylindrical object with respect to the palm of a hand to determine the ability to successfully grasp this object. Palm position is represented by the solid object and the pinch position by the dashed object. D_{obj} is the diameter of the object, $2L_0$ is the width of the palm, L_1 is the length of the proximal phalanx, L_2 is the length of the distal phalanx, L is the length of the finger. A torque Ta applies to the base of the fingers.

attached at the cylinder center. The apparatus was oriented such that it was symmetric with the fingers and the load cell measured the force exerted between the opposing fingers in the direction of the split. The same test artifact was used to measure both power grasping (Figure 33 - Left) and finger-tip grasping (Figure 33 - Right).

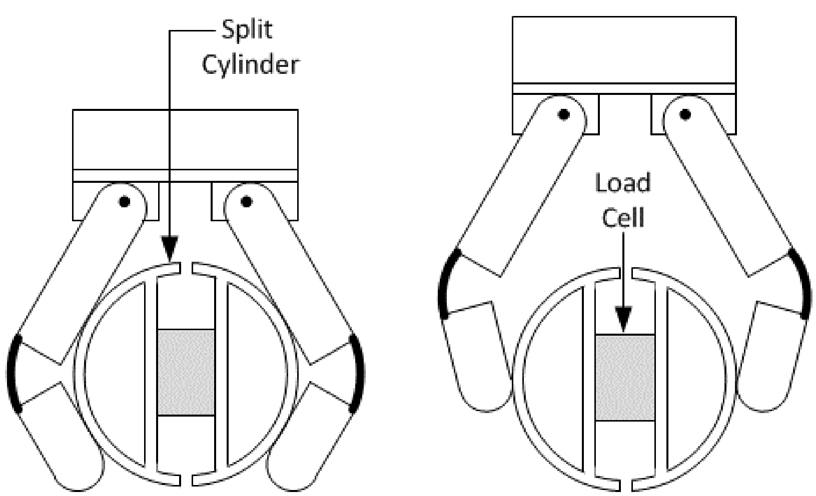

Fig. 33. Reproduced from [2] split ring test apparatus to measure power grasp and finger- tip force.

Romano et al. [10] presents quantitative testing when evaluating the performance of a novel robotic grasp controller. The system's ability to control delicate manipulation tasks was evaluated with crushing measures. Crushing was defined as a deformation of 10 mm beyond the initial surface contact. There was no indication as to how these measurements were made.

A.4 Resistance to Force and Slip

A benchmark in [1] tests the ability to hold objects. Again using cylindrical objects, the object is placed against the palm of the hand and grasped. The object is slowly moved along a straight line (5 mm/s) in a disturbance direction μ, with the object allowed to move in the perpendicular direction ν (Figure 34). The force is measured throughout the pulling direction over several pull directions Φ and the maximum pull force is recorded for each. A performance metric was designed as follows:

$$Q_{hold} = \frac{FL}{T_a}, \tag{13}$$

where F is the minimum force needed to pull an object out of the hand, T_a is the constant actuation torque applied at the base of the fingers, and L is the total length of the finger. In [11] the authors conduct similar experiments with grasps as in [1] but also independently measure the contact force using a load cell internal to the cylinder and coupled to the hand though a ball bearing protruding through a hole in the cylinder. In these tests, the authors are relating the forces exerted on the cylinder by the hand to the forces required to pull the cylinders from the hand.

Romano et al. [10] test a robotic hand's ability to control delicate manipulation tasks using slippage measures. Slippage was defined in two forms: translation (greater than 5 mm), and rotation (greater than 10 degrees). There was no indication as to how these thresholds were developed. Slip measures were used to evaluate the grasp controller's ability to adjust the minimum grip force necessary to lift an object 10 mm from a table surface and to evaluate the controller's slip response. To evaluate slip response, a cup was stably grasped at a fixed load of 5N. The cup was loaded incrementally with batches of 15 marbles (about 0.6 N per batch) and the gripper was shaken for two seconds while the cup was observed for slip. The authors also used pressure-sensitive film to capture the forces imposed on an object during placement onto a flat surface.

A.5 Touch Sensitivity

Dollar et al. [12] presents an experimental setup to test grasp improvements achieved when integrating piezofilm contact sensors with a reactive control algorithm onto the Shape Deposition Manufactured (SDM) Hand. The experimental setup consists of a shape artifact constrained to a six-axis force-torque sensor. A nominal grasp pose relative to the position of the artifact to be grasped is determined. Error offsets are then applied to the nominal

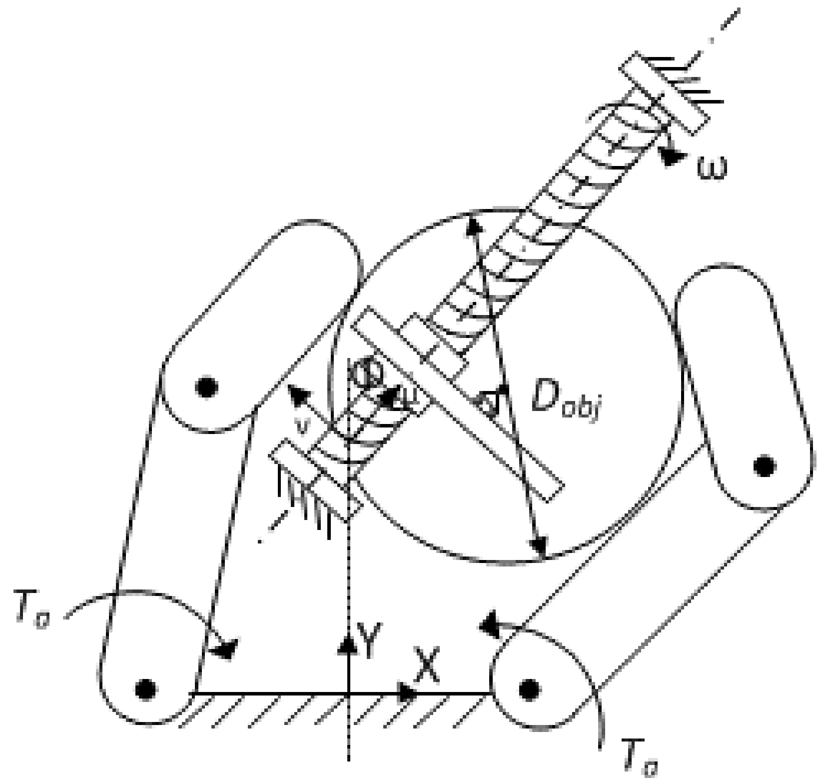

Fig. 34. Reproduced from [1], a schematic for the setup where a cylindrical object with a diameter D_{obj} is pulled out of the hand at a constant slow speed ω in the direction of μ while the fingers are at a constant torque Ta. The object is free to move in the direction v, which is perpendicular to μ. The resultant of the contact forces on the object in the pull direction μ is measured.

pose and the forces associated with and without sensor based feedback improvements are measured. In addition to the force measurements, a qualitative assessment is applied to measure the success of the grasp. A successful grasp is defined as one where the object is able to be successfully lifted out of the force sensor mount without slipping out of the hand. In the reported experiments, grasp success and contact force data were evaluated at 10 mm error increments from the nominal position and showed that the addition of feedback from the contact sensors on the hand decreased the forces applied to the object during the grasp and increased the range of acceptable positioning offsets that still resulted in a successful grasp.

Based on Dollar's work, SynTouch LLC reports an experiment for comparing the sensitivity of grasp using tactile sensing technologies. Using a spherical object fixed to a force plate, the experiment measures the unbalanced forces acting on the object upon making grasp point contacts. The tests were conducted over a range of closing velocities and varied the position of the object to test how grasps can adapt to positional errors. Results showed higher forces with increasing closing velocities and decreasing sensor compliance and were attributed to the speed of the hand's force control loop using the integrated sensor system. The research also presented a mechanism for using the collected data to determine the range of velocities and position errors a robotic hand system can tolerate for a given peak force.

A.6 Compliance

The developers of the iHY also developed a test for measuring the compliance of planar and spherical pinch grasps [2]. This was accomplished by mounting a 6-axis force-torque sensor to a mill headstock with the iHY hand fixtured in the mill's vice (Figure 35). Disturbance displacements were applied using the three linear axis of the milling machine, and the resultant forces were recorded relative to displacement. Stiffness values were determined by averaging out hysteresis due to tendon friction and the viscoelasticity of polymer pads and flexures by averaging values in both directions of each motion over several cycles. A linear least squares estimation was used to fit the parameters of a symmetric stiffness matrix **K** to the data for both the opposed and spherical fingertip grasps.

$$K = \begin{bmatrix} K_{xx} & K_{xy} & K_{xz} \\ K_{yx} & K_{yy} & K_{yz} \\ K_{zx} & K_{zy} & K_{zz} \end{bmatrix} \tag{14}$$

A.7 In-Hand Manipulation

Odhner et al. [13] reports on experiments used to evaluate the in-hand manipulation capabilities using two fingers of an under-actuated robotic hand. Using several small objects having different width and radius of curvature, manipulation tests were conducted by tracking the position of the object relative to an initial fingertip grasped position. Objects were tracked in six degree-of-freedom space using a commercially available tracking system and the degree of slip was detected by measuring the error between the nominal start and finish object positions after returning the robotic hand fingers to their original fingertip grasp position.

A.8 Grasp Properties and Quantitative Measures

Grasp synthesis identifies the physical and mechanical properties of grasps and the creation of suitable parameters to quantify them. In a review of grasp synthesis algorithms, Shimoga identifies the main properties of grasp as disturbance resistance, dexterity, equilibrium, stability, and dynamic behavior [14]. A grasp with good disturbance resistance can withstand disturbances in any direction. This can be accomplished by form-closure (complete kinematical restraint) where a set of grasp points results in finger positioning that constrains an object, or force closure where grasp point forces applied by fingers constrain motion of

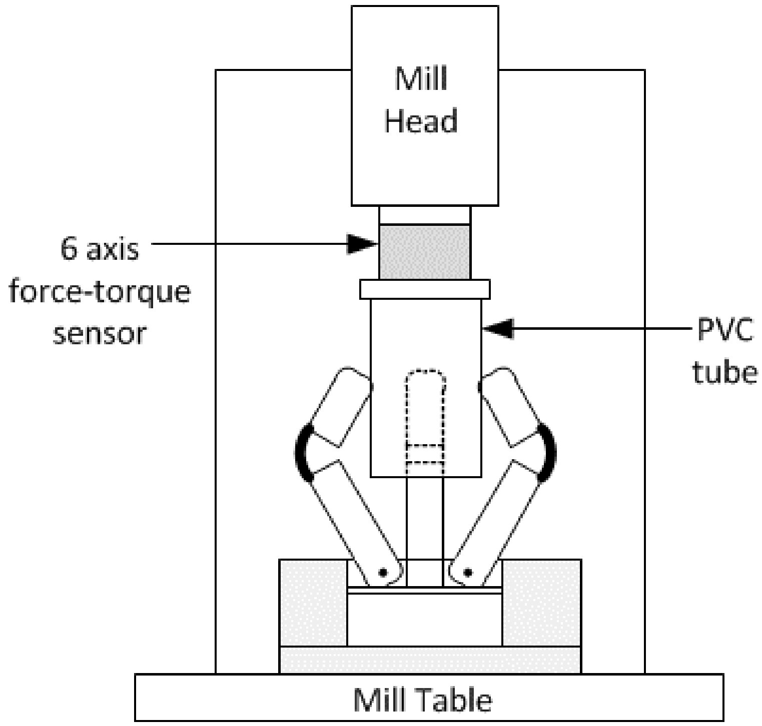

Fig. 35. Reproduced from [2], experimental setup for measuring stiffness properties of compliant hand

the object (specific measures for these are proposed by many researchers and are discussed in Section 5.3). A grasp is considered dexterous if the kinematic properties of the robotic hand allow the object to be moved using a controlled and stable method, a concept also referred to as in-hand manipulation. A grasp is in equilibrium if resultant forces and torques applied to an object by finger and external forces equate to zero. A grasp is considered to be stable if any positional errors caused by external forces in finger or object position can be eliminated once the disturbance is removed. Finally, the dynamic behavior of a grasp is defined as the time response of the grasp for changes in its motion or force trajectories.

Similar to Shimoga, Cutkosky presents the properties of force closure, form closure, stability, and manipulability as analytical measures used to describe a grasp [5]. Cutkosky also presents internal forces, slip resistance, compliance, and connectivity. Internal forces apply to the magnitude and variance of forces that a hand applies to an object while maintaining grasp equilibrium that is described above. Slip resistance is the magnitude of the forces and moments on the object at the onset of slip. The resistance to slipping depends on the configuration of the grasp, on the types of contacts, and on the friction between the object and the fingertips. Compliance (inverse of stiffness) of the grasped object with respect to the hand is a function of grasp configuration, joint servoing, and structural compliances in the links, joints, and fingertips. Finally, connectivity is the number of degrees of freedom

Table 9. Grasp properties and applicable performance tests

Grasp Property	Description	Applicable Tests (Appendix A section)
Form Closure	Ability to spatially constrain an object from moving when the finger joints are locked when assuming contact between the fingers and the object.	A.2
Force Closure	There exists a conical combination of contact forces at the points of contact such that any external wrench applied to the object can be resisted.	A.3, A.4
Manipulability	The ability of the fingers to impart motions to the object using the kinematic properties of the robotic hand allowing the object to be moved using a controlled and stable method. Also called in-hand manipulation.	A.7
Equilibrium	Resultant forces and torques applied to an object by finger and external forces equate to zero	A.3, A.4
Stability	Ability of the grasp to return to its initial configuration after being disturbed by an external force or moment.	none
Dynamic Behavior	The time response of the grasp for changes in its motion or force trajectories.	none
Internal Forces	Magnitude and variance of internal grasp forces that a hand applies to an object without disturbing the grasp equilibrium.	A.3
Slip	Magnitude of the forces and moments on the object at the onset of slip.	A.4
Compliance	The effective compliance of the grasped object with respect to the hand.	A.6
Connectivity	Number of degrees of freedom between the grasped object and the hand.	A.7
Sensitivity	Ability to conform to deviations in nominal object position without disturbing actual object location prior to achieving final grasp.	A.5

between the grasped object with respect to the hand.

Another important property as indicated in [8] that we will call grasp sensitivity, is the ability of a grasp to conform to deviations in nominal object position without disturbing actual object location prior to achieving form closure with the object. Grasp sensitivity is a property of a force or contact sensing and associated control algorithms that occurs when achieving form closure. Table 9 consolidates these measures and maps them to the quantitative experimental methods as described in the first part of this report. As indicated, there are multiple performance tests that can be used to assess a given measure; and some measures can be supported using several of the experimental methods found in the literature.

Appendix B: Analysis of a Grasping Task

Breaking down a problem into its parts can provide novel insights towards its solution. Consider the underlying tasks associated with a robotic pick and place operation for a fully integrated multi-fingered robotic hand (see Figure 36). Each task in this operation possesses several associated problems that can serve as a basis for extracting performance measures. More specifically, quantifying the performance of a system in handling these problems can help guide and justify the various strategies taken. Furthermore, identifying the significance of performance measures towards different grasping tasks would provide valuable knowledge on necessary functionalities and their performance towards task completion. For example, picking up a part and tossing it into a bin requires minimal position accuracy of the grasped object once the grasp component is completed, where picking up a part and performing an assembly operation requires much more accurate positioning throughout the task. Thus, quantifying and suggesting a minimal level of performance in the system's ability to control and measure object position in the latter scenario would be critical in predicting operation success.

A plausible outline for the pick and place operation begins with a "best" set of grasp points as determined from a grasp planner. The hand is positioned by a robotic arm to cage an object by establishing an approach trajectory and offsets that are based on the grasp planning stage. During the cage task segment, it is possible for components of the robotic hand to run into obstructions near the object or run into the candidate object to be grasped due to inadequate clearances.

During the constrain task segment, the object is spatially confined by the grasp at the grasp points. Sensorless contacts depend on the positioning accuracy of the hand delivery system and/or the synchronization of fingertip position in time. Unsynchronized contact requires minimal force contacts to minimize disturbance to the part, if maintaining part position is important, and requires hand sensing capabilities such as tactile or current sensing. Position problems can occur during this task segment that result in a missed contact point where the part is not fully constrained and contact movement due to synchronization issues or inadvertent contact by the hand due to clearance issues. Clearance issues may also result if the object is too small to be grasped as in the case of a 3-fingered radial grasp on a cylinder where closing the fingers results in a collision between fingers before contacting the object.

The load task segment applies the calculated forces required to keep a firm grasp on the object. These forces are most often calculated to obtain an efficient grasp based on the forces required to stabilize the object in the presence of gravitational and inertial forces. Problems during this segment are due to the uncertainty in the kinetics of the system (i.e., object mass), disturbance forces, and torques applied to the object. Uncertainty in the system can lead to the occurrence of slippage, damage to the part (crushing), or ejection when trying to achieve efficient grasp forces.

The pick task segment lifts the object for manipulation. Problems during this segment are due to the errors between gravitational forces and the forces applied during the load task and again result in slippage, ejection or crushing. Other considerations are variations in object position relative to the robot hand coordinate frame upon picking up the part due to the compliance properties of the robot hand.

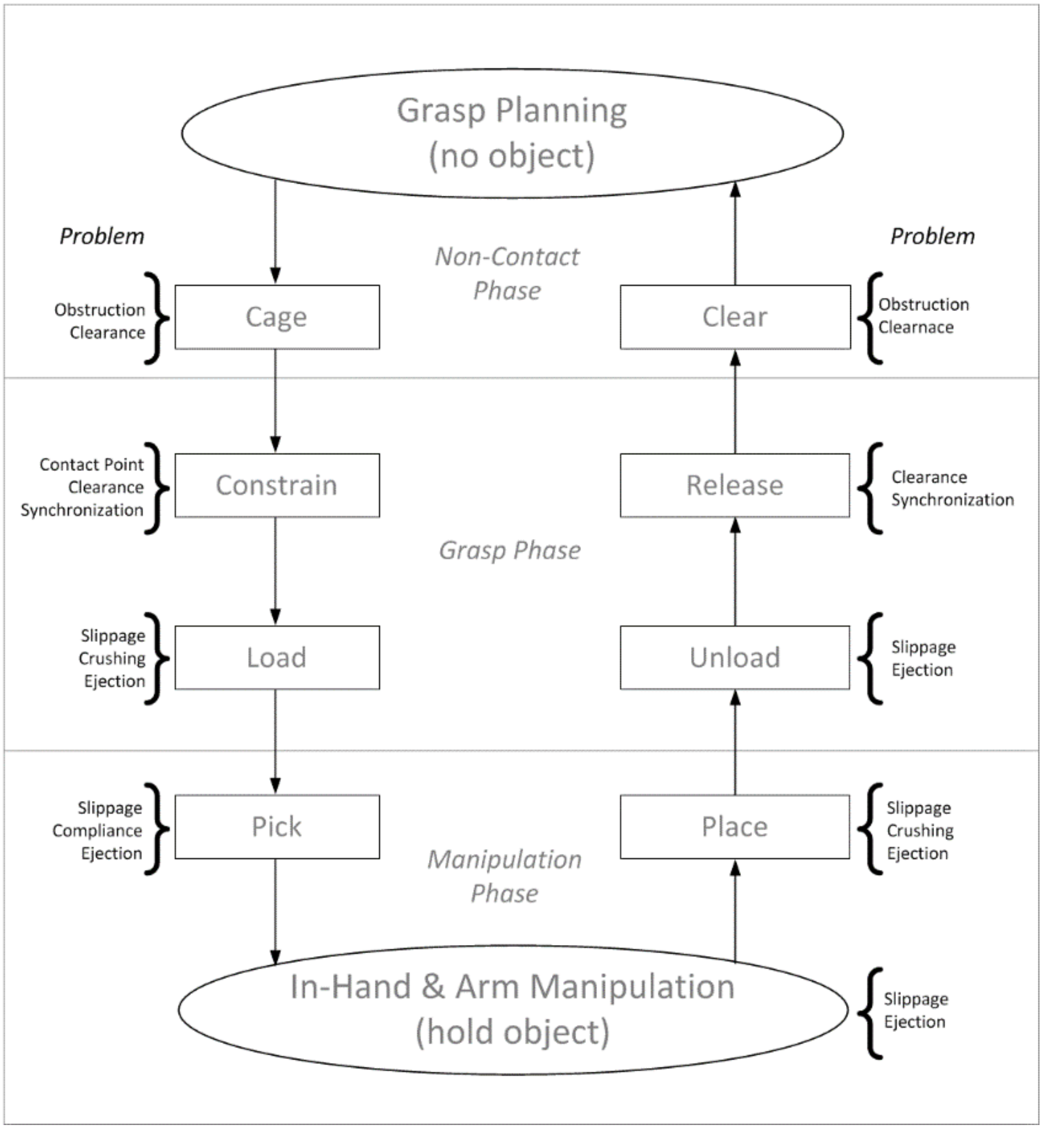

Fig. 36. Pick and place task segmentation and transitions between grasped and un-grasped states

During the manipulation phase, the part is picked (or lifted) from its grasped position, moved along a trajectory, and placed in a final position. The trajectory could be induced by the robot carrying the hand as well as the robotic hand itself, often referred to as in-hand manipulation. Problems are due to change in part position relative to the hand caused by external forces associated with contacts between the object and the environment throughout the manipulation process as well as uncertainty in the object's kinetic properties. In addition, fluctuations in the mass of the object as well as exogenous disturbances can occur due to an intermediate assembly operation on the object. These force changes can result in slippage, ejection, or crushing.

During the place task segment the object errors are dependent on object positional placement accuracy. In the most lenient case, the object is to be placed into a bin at a random orientation. In another case the object is positioned on a flat surface where accuracy errors could result in unexpected surface/object contact forces leading to ejection, slip, or crushing. The most complex case is that of assembly where assembly algorithms are dependent on the positional accuracy of initial contact between the object and the subassembly and the object is subjected to a multitude of external forces throughout the assembly process also leading to ejection, slip, or crushing.

Post manipulation phase, the remaining task segments are a reversal of the task segments that lead up to the manipulation phase and the errors associated with these are like their counterparts. Here the object is unloaded to the point of zero force contact and released so that the robot hand components clear the object allowing the hand to be moved to the next operation.

Appendix C: Test Artifacts

The split cylinder artifacts support the grasp strength, slip resistance, and grasp efficiency NIST elemental grasp performance test methods. The cylinder artifacts incorporate ASTM D2665 PVC pipe for the following reasons: 1) the cylindrical pipe comes in a variety of standard diameters with dimensions that are compatible with robot hand volumetric capabilities, and 2) the surface properties of these pipes are relatively consistent. A 304.8 mm (12 in) segment of PVC pipe is cut in half along the axial direction. Each PVC pipe half is then glued to the two pipe cores using epoxy resin. The primary alignment of the plastic cores is accomplished using two 4 mm diameter dowel pins where the pin holes in the 3D printed core are drilled to achieve a slip fit. Figure 37 and Figure 38 show the 50.4 mm (2 in) inner diameter PVC split cylinder designs using single axis load cells and the resistive force sensor force measurement techniques, respectively. Figure 39 shows the 76.2 mm (3 in) PVC pipe configuration where two additional sensors are added to stabilize the axial forces. More information regarding the design of these artifacts can be found on the NIST Performance Metrics and Benchmarks to Advance the State of Robotic Grasping website [15]

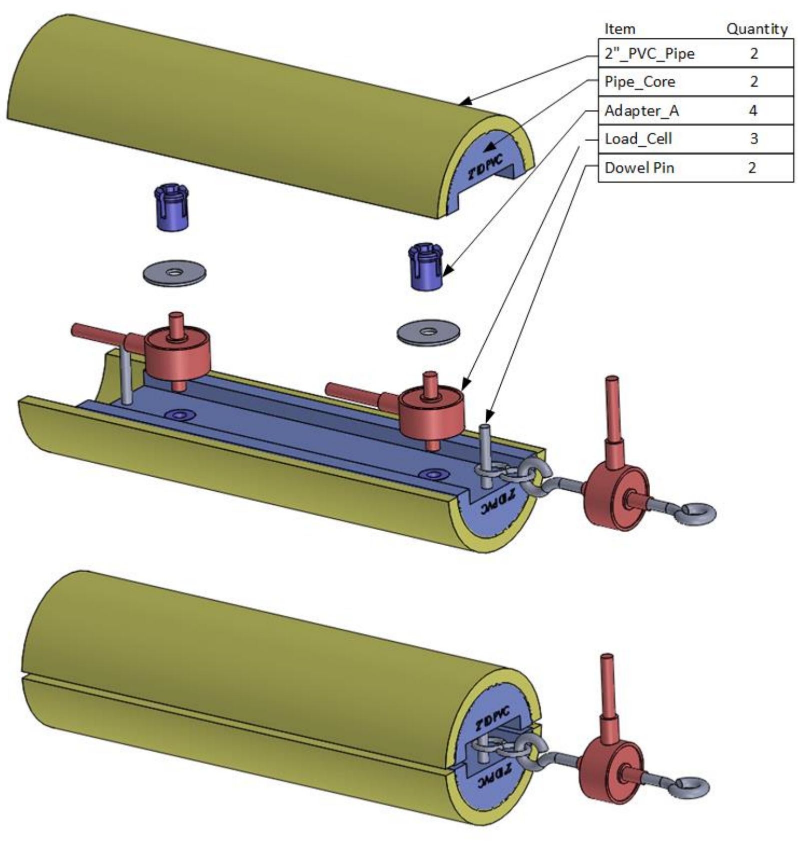

Fig. 37. 50.4 mm (2 in) ID PVC Split Cylinder Artifact with Single Axis Load Cells

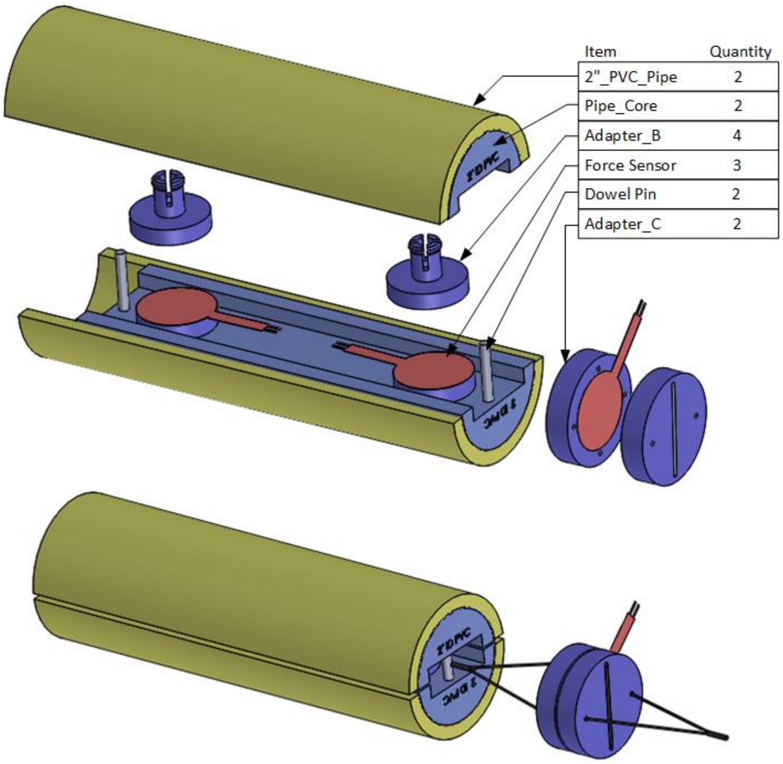

Fig. 38. 50.4 mm (2 in) ID PVC Split Cylinder Artifact with Low Cost Force Sensitive Resistors

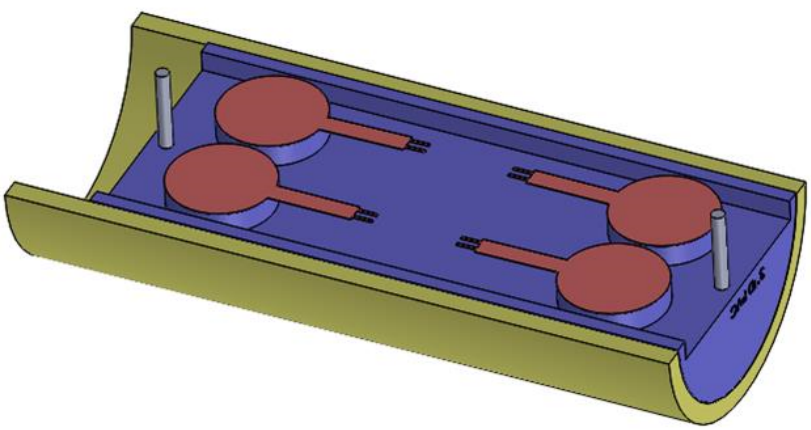

Fig. 39. 76.2 mm (3 in) ID PVC Split Cylinder Artifact Half with Low Cost Force Sensitive Resistors

Appendix D: Determining Test Method Sample Size

Pass-Fail Data

To determine the required sample size (n) for pass-fail test data, one can use the following equation,

$$n = \frac{ln(1-CL)}{ln(PS)}, \tag{15}$$

where CL is the desired confidence level (typically 0.95), and PS is the desired probability of success [16]. This formulation assumes that failures do not occur within n number of trials. Example values are shown in Table 10.

		Probability of Success					
		0.85	**0.90**	**0.95**	**0.987**	**0.99**	**0.9999966**
Confidence Level	**0.85**	12	19	37	150	189	557976
	0.90	15	22	45	182	230	677230
	0.95	19	29	59	236	299	881097
	0.99	29	44	90	363	459	1354460

Table 10. Minimum samples required to establish probabilities of success at confidence intervals.

If failures occur during testing, then one can update the calculation of PS as follows. Given a confidence level $CL \in \mathbb{R} : [0,1]$, number of successes m, and number of independent trials n, one can calculate the theoretical probability of success $PS \in \mathbb{R} : [0,1]$ from the following inequality involving the binomial cumulative distribution function,

$$BINCDF(m-1, n, PS) \geq CL, \tag{16}$$

where PS is its minimum value to some precision while still satisfying (16). Alternatively, one can use (16) with parameter settings of PS, CL, and m to calculate the number of required samples n.

Continuous Data

To determine sample size for continuous test data, a common strategy involves analyzing sample means. For instance, one can set the tolerable error δ in calculating the true system performance average μ with the following relationship

$$\bar{X} - \delta \leq \mu \leq \bar{X} + \delta, \tag{17}$$

where $\bar{X}$ is the sample average [17]. Ideally, the population standard deviation σ should also be known, but is very often unknown. Alternatively, the sample standard deviation s could be used, but is also not known in advance unless preliminary or past experiments have already been conducted. Therefore, assuming that a sample standard deviation is not known, a general strategy is to conduct a few experiments first (e.g., ten trials) and then calculate the remaining number of trials required. Once an initial sample standard devation s is known, one can use the following equation to calculate the number of required trials n for a two-sided test,

$$n = (t_{1-\alpha/2} + t_{1-\beta})^2 (\frac{s}{\delta})^2, \tag{18}$$

where $t_{1-\alpha/2}$ and $t_{1-\beta}$ are critical values of the t-distribution with the degrees of freedom equal to n-1 from the initial sample set (e.g., ten trials). α (typically 0.05) is 1-CL is the likelihood of falsely rejecting the null hypothesis, while β (typically 0.1-0.2) is the likelihood of falsely accepting the null hypothesis. Alternatively, δ can be expressed in terms of σ for simplicity (e.g., $\delta = 1.0\sigma$). With this route, an example table of sample sizes can be calculated in advance as in Table 11 (reproduced from [17])

α	β	δ=0.5σ	δ=1.0σ	δ=1.5σ
0.01	0.01	98	25	11
0.01	0.05	73	18	8
0.01	0.10	61	15	7
0.01	0.20	47	12	6
0.01	0.50	27	7	3
0.05	0.01	75	19	9
0.05	0.05	53	13	6
0.05	0.10	43	11	5
0.05	0.20	33	8	4
0.05	0.50	16	4	3
0.10	0.01	65	16	8
0.10	0.05	45	11	5
0.10	0.10	35	9	4
0.10	0.20	25	7	3
0.10	0.50	11	3	3
0.20	0.01	53	14	6
0.20	0.05	35	9	4
0.20	0.10	27	7	3
0.20	0.20	19	5	3
0.20	0.50	7	3	3

Table 11. Minimum samples required to establish tolerable error of mean δ with preset confidence (α) and power levels (β).

References

[1] Kragten GA, Meijneke C, Herder JL (2010) A proposal for benchmark tests for underactuated or compliant hands. *Mechanical Sciences* 1(1):13–18.

[2] Odhner LU, et al. (2014) A compliant, underactuated hand for robust manipulation. *The International Journal of Robotics Research* 33(5):736–752.

[3] Deshpande AD, et al. (2013) Mechanisms of the anatomically correct testbed hand. *IEEE/ASME Transactions on Mechatronics* 18(1):238–250.

[4] Controzzi M, Cipriani C, Carrozza M (2014) *The Human Hand as an Inspiration for Robot Hand Development* (Springer International Publishing), Vol. 95, Chapter 2, , pp 219–246.

[5] Cutkosky M (1989) On grasp choice, grasp models, and the design of hands for manufacturing tasks. *IEEE Transactions on Robotics and Automation* 5(3):269–279.

[6] Feix T, Pawlik R, Schmiedmayer H, Romero J, Kragic D (2009) A comprehensive grasp taxonomy. *Robotics, Science and Systems: Workshop on Understanding the Human Hand for Advancing Robotic Manipulation*, .

[7] DARPA Robot Challenge, https://www.darpa.mil/program/darpa-robotics-challenge. Access Date: 07/26/2018.

[8] DARPA Arm Challenge, https://www.darpa.mil/program/autonomous-robotic-manipulation. Access Date: 07/26/2018.

[9] Guide for evaluating, purchasing, and training with response robots using dhs-nist-astm international standard test methods, http://www.nist.gov/el/isd/ms/upload/DHS_NIST_ASTM_Robot_Test_Methods-2.pdf. Access Date: 07/26/2018.

[10] Romano JM, Hsiao K, Niemeyer G, Chitta S, Kuchenbecker KJ (2011) Human-inspired robotic grasp control with tactile sensing. *IEEE Transactions on Robotics* 27(6):1067–1079.

[11] Meijneke C, Kragten GA, Wisse M (2011) Design and performance assessment of an underactuated hand for industrial applications. *Mechanical Sciences* 2(1):9–15.

[12] Dollar AM, Jentoft LP, Gao JH, Howe RD (2009) Contact sensing and grasping performance of compliant hands. *Autonomous Robots* 28(1):65.

[13] Odhner LU, Ma RR, Dollar AM (2013) *Experiments in Underactuated In-Hand Manipulation* (Springer International Publishing, Heidelberg), , , , pp 27–40.

[14] Shimoga K (1996) Robot grasp synthesis algorithms: A survey. *The International Journal of Robotics Research* 15(3):230–266.

[15] Performance metrics and benchmarks to advance the state of robotic grasping, https://www.nist.gov/el/intelligent-systems-division-73500/robotic-grasping-and-manipulation-assembly/grasping. Access Date: 07/26/2018.

[16] Gilliam D, Leigh S, Rukhin A, Strawderman W (2009) Pass-fail testing: Statistical requirements and interpretations. *Journal of research of the National Institute of Standards and Technology* 114(3):195.

[17] (2018) Nist/sematech e-handbook of statistical methods, https://www.itl.nist.gov/div898/handbook/prc/section2/prc222.htm. Access Date: 07/26/2018.